AD-A187 185 ON STRESS COLLAPSE IN ADIABATIC SHEAR BANDS(U) ARMY BALLISTIC RESEARCH LAB ABERDEEN PROVING GROUND MD T W WRIGHT ET AL. JUN 87 BRL-TR-2816 1/1

UNCLASSIFIED F/G 20/11 NL

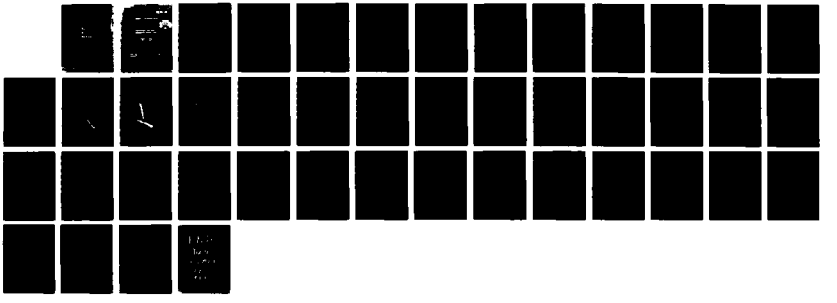

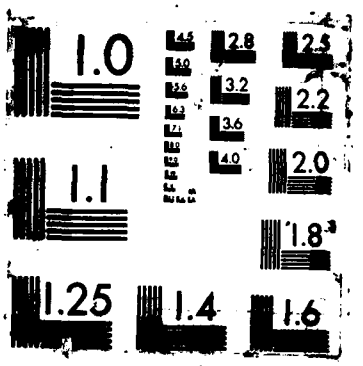
1.0
1.1
1.25
1.4
1.6
1.8
2.0
2.2
2.5
2.8
3.2
3.6
4.0

AD

TECHNICAL REPORT BRL-TR-2818

ON STRESS COLLAPSE IN ADIABATIC SHEAR BANDS.

THOMAS W. WRIGHT
JOHN W. WALTER

JUNE 1987

US ARMY BALLISTIC RESEARCH LABORATORY
ABERDEEN PROVING GROUND, MARYLAND

DESTRUCTION NOTICE

Destroy this report when it is no longer needed. DO NOT return it to the originator.

Additional copies of this report may be obtained from the National Technical Information Service, U.S. Department of Commerce, Springfield, VA 22161.

The findings of this report are not to be construed as an official Department of the Army position, unless so designated by other authorized documents.

The use of trade names or manufacturers' names in this report does not constitute indorsement of any commercial product.

UNCLASSIFIED
SECURITY CLASSIFICATION OF THIS PAGE

REPORT DOCUMENTATION PAGE

Form Approved
OMB No 0704-0188
Exp Date Jun 30, 1986

1a. REPORT SECURITY CLASSIFICATION Unclassified	1b. RESTRICTIVE MARKINGS
2a. SECURITY CLASSIFICATION AUTHORITY	3. DISTRIBUTION/AVAILABILITY OF REPORT Approved for public release; distribution unlimited
2b. DECLASSIFICATION/DOWNGRADING SCHEDULE	
4. PERFORMING ORGANIZATION REPORT NUMBER(S)	5. MONITORING ORGANIZATION REPORT NUMBER(S)
6a. NAME OF PERFORMING ORGANIZATION Ballistic Research Laboratory 6b. OFFICE SYMBOL (If applicable) SLCBR-TB-W	7a. NAME OF MONITORING ORGANIZATION
6c. ADDRESS (City, State, and ZIP Code) Aberdeen Proving Ground, MD 21005-5066	7b. ADDRESS (City, State, and ZIP Code)
8a. NAME OF FUNDING/SPONSORING ORGANIZATION 8b. OFFICE SYMBOL (If applicable)	9. PROCUREMENT INSTRUMENT IDENTIFICATION NUMBER
8c. ADDRESS (City, State, and ZIP Code)	10. SOURCE OF FUNDING NUMBERS PROGRAM ELEMENT NO. / PROJECT NO. / TASK NO. / WORK UNIT ACCESSION NO
11. TITLE (Include Security Classification) On Stress Collapse in Adiabatic Shear Band	
12. PERSONAL AUTHOR(S) Thomas W. Wright and John W. Walter	
13a. TYPE OF REPORT Final 13b. TIME COVERED FROM _____ TO _____	14. DATE OF REPORT (Year, Month, Day) 15. PAGE COUNT
16. SUPPLEMENTARY NOTATION	
17. COSATI CODES FIELD / GROUP / SUB-GROUP	18. SUBJECT TERMS (Continue on reverse if necessary and identify by block number)

19. ABSTRACT (Continue on reverse if necessary and identify by block number)

The dynamics of adiabatic shear band formation is considered making use of a simplified thermo/visco/plastic flow law. A new numerical solution is used to follow the growth of a perturbation from initiation, through early growth and severe localization, to a slowly varying terminal configuration. Asymptotic analyses predict the early and late stage patterns, but the timing and structure of the abrupt transition to severe localization can only be studied numerically, to date. A characteristic feature of the process is that temperature and plastic strain rate begin to localize immediately, but only slowly, whereas the stress first evolves almost as if there were no perturbation, but then collapses rapidly when severe localization occurs.

20. DISTRIBUTION/AVAILABILITY OF ABSTRACT ☐ UNCLASSIFIED/UNLIMITED ☒ SAME AS RPT ☐ DTIC USERS	21. ABSTRACT SECURITY CLASSIFICATION Unclassified
22a. NAME OF RESPONSIBLE INDIVIDUAL Thomas W. Wright	22b. TELEPHONE (Include Area Code) 301-278-6046 22c. OFFICE SYMBOL SLCBR-TB-W

DD FORM 1473, 84 MAR

83 APR edition may be used until exhausted
All other editions are obsolete

SECURITY CLASSIFICATION OF THIS PAGE
UNCLASSIFIED

ACKNOWLEDGMENT

The authors are grateful to Prof. J. W. Hutchinson for calling their attention to the paper on necking in a viscoplastic material.

LIST OF FIGURES

LIST OF FIGURES

TABLE OF CONTENTS

1. INTRODUCTION

Localized deformation tends to occur in materials whenever a mechanism develops that permits strain softening. The most familiar example is necking in a ductile tension specimen where the required mechanism is area reduction in the cross section. An adiabatic shear band can form in a ductile material when thermal softening, due to heat generated by plastic deformation, is stronger than strain hardening, strain rate hardening, and all other hardening mechanisms combined. The basic phenomenon was pointed out by Zener and Holloman[1] and in recent years there has been substantial renewed interest in an analytical treatment. A general result found by several authors (e.g., Rubin and Drucker,[2] Clifton,[3] Clifton, et al.[4] Bai,[5] Burns[6] is that localization cannot begin until the stress in the corresponding homogeneous deformation passes a maximum. It has also been observed that the predicted subsequent rate of growth of inhomogeneities is insufficient to explain observed dynamic stress-strain curves, even though the predicted strain at peak homogeneous stress may be quite accurate.

In a series of papers Wright and Batra[7 8 9] considered the problem of shear band formation around a small initial perturbation in one dimension by performing a fully nonlinear finite element calculation. They found that although the fields for both temperature and strain rate did begin to localize slowly near the stress maximum, the calculated stress, which remained nearly constant in space, followed the homogeneous stress for some time after peak stress, and then dropped rapidly. Furthermore, the localization in both temperature and strain rate accelerated sharply as stress collapse began and the time of collapse depended on the size of the initial perturbation. These results are summarized pictorially in Figure 1.

Unfortunately, the calculation became unstable just as the stress drop was getting underway so that the validity of the result remained in doubt, and the full morphology of the completed band could not be calculated. In other fully nonlinear calculations, Clifton, et al.[4] did not continue far enough to observe the stress drop, but Merzer[10] did in one example, although the constitutive equations used in the latter case were quite different from those used by Wright and Batra.[7 8 9] Thus there seemed to be evidence that the two stage process of localization is quite general.

In most cases the loss of strength is of much greater significance than the mere fact of localization in the deformation or temperature. Furthermore, in dynamical problems the timing of events is usually crucial. Therefore, in many applications it is important to understand the transitional nature of localization in far greater detail than heretofore.

In this paper, so that mathematical details will be as transparent as possible without obscuring the physical phenomena, a minimalist version of thermo/visco/plasticity is used to formulate a localization problem. Both the unsteady homogeneous solution and the first order perturbation solution for arbitrary initial conditions can then be found explicitly. The analysis shows that the stress perturbation does not grow to first order, even though the temperature and strain rate perturbations grow exponentially. A byproduct of the perturbation solution is a criterion for absolute stability, which also yields the least plastic strain rate at which shear bands

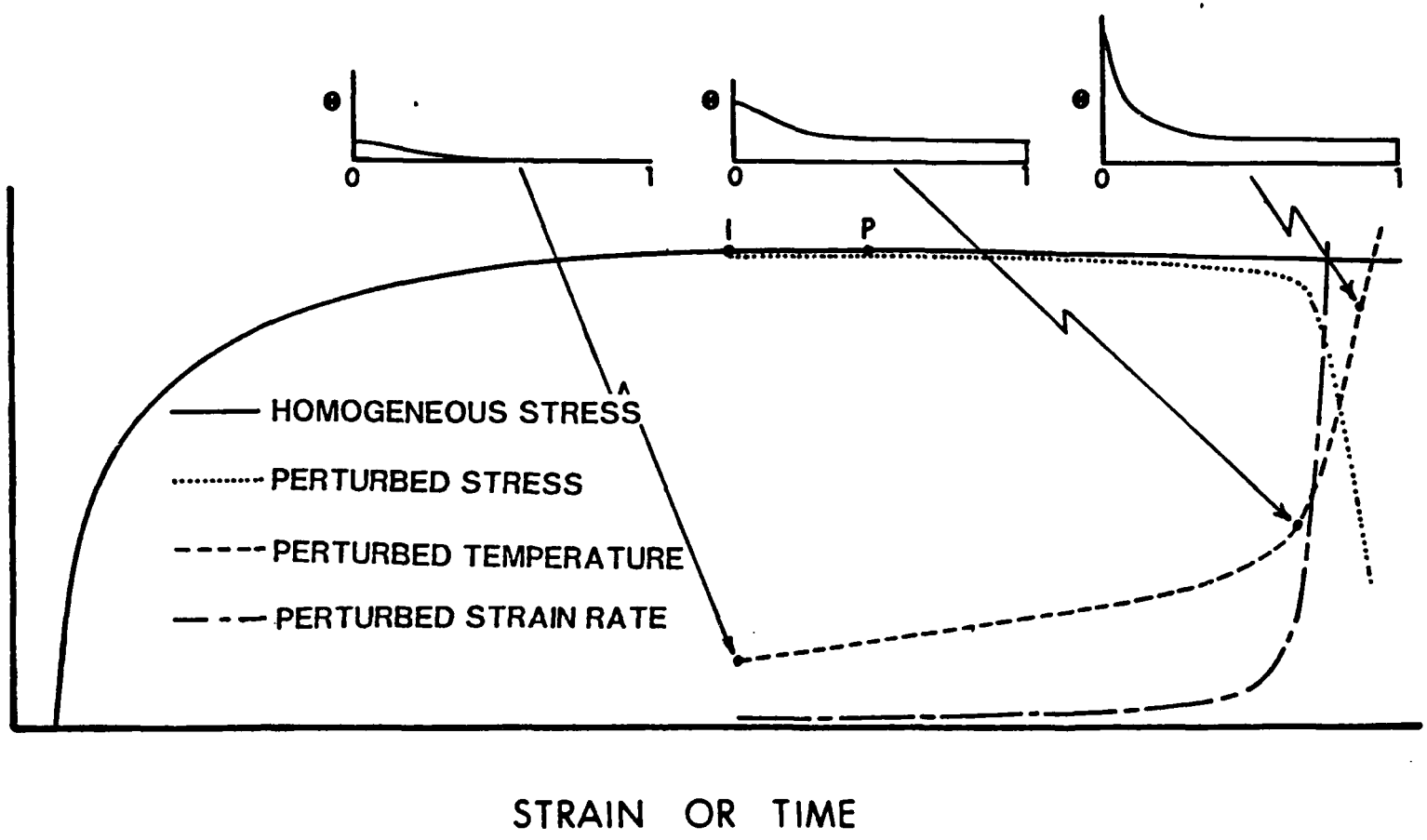

Figure 1. Sketch showing the evolution of stress, maximum temperature, and maximum strain rate, when a small temperature perturbation is introduced just before peak stress.

can form. A new numerical anaysis, which is stable through all the rapid transition regions, confirms the accuracy of the perturbation solution at early times as well as the accuracy of the stability criterion. Furthermore, it is demonstrated that there is a rapid transition region where the stress drops sharply, and for the first time, a stable calculation has been made that fully resolves all the spatial details of the localization and that also follows the process all the way to the terminal configuration. At the end of the calculation the plastic strain rate has reached a plateau in the center of the band, and, in fact, its spatial distribution has become completely independent of time. A previous steady analysis, Wright,[11] predicts this distribution with great accuracy, so that the present calculation confirms the previous conjecture that the steady solutions represent the core of a shear band as a central boundary layer. A new quasi-steady analysis also gives the terminal configuration for plastic strain rate, but now it is completely determined for a given material once the applied strain rate is specified, and it is totally independent of the nature of the initial perturbation.

Thus, many details concerning the formation of adiabatic shear bands have been fully explained, with analysis and computation in complete agreement with each oher, at least for the constitutive relations used here. One aspect of localization, which is crucial for dynamical problems, remains obscure, namely, a full understanding of the timing of the abrupt collapse in stress. Parametric calculations with a triangular initial perturbation indicate that the time of collapse depends strongly on the area of the triangle, but only weakly on the slope of the sides. These results seem to be in accord with expectations based on the stability criterion, but an asymptotic analysis that predicts the time of collapse remains elusive.

2. FORMULATION OF PROBLEM AND HOMOGENEOUS SOLUTIONS

The problem to be studied is simple shear of a finite slab of incompressible material, which is further assumed to be rigid/perfectly plastic in slow isothermal deformation, to be rate dependent, and to soften with increasing temperature. The boundaries will be prescribed to be thermally insulated and to move at constant velocity. Heat conduction and heat generation due to plastic work will be taken into account, and the initial conditions will be assumed to be nearly uniform in temperature and plastic strain rate.

With the X material coordinate taken parallel to the boundary and in the direction of shearing, and with the Y material coordinate taken perpendicular to the boundary, the motion may be written as

$$x = X + u(Y,t) \quad , \quad y = Y \quad , \quad z = Z \tag{1}$$

where u is displacement and t is time. In nondimensional form, with $-1 \leq Y \leq +1$ and $0 \leq t < \infty$, the governing balance and constitutive equations are given by

$$\begin{aligned} &\text{Momentum:} && s_{,y} = \rho v_{,t} \\ &\text{Energy:} && \theta_{,t} = k\theta_{,yy} + s v_{,y} \\ &\text{Flow Law:} && s = (1 - a\theta)(1 + b v_{,y})^{m}. \end{aligned} \tag{2}$$

In these equations the dependent variables are the shear stress s, velocity $v = u_{,t}$ and temperature θ, which is assumed to be measured from a convenient reference temperature. Commas denote partial differentiation with respect to the independent variable indicated. The material parameters ρ, k, a, b, and m are nondimensional constants, and stand respectively for nondimensional density, thermal conductivity, thermal softening coefficient, characteristic time in the Litonski flow law, and the rate hardening exponent. The relationships between the nondimensional and dimensional (barred) quantities are as follows.

$$\begin{aligned} &y = \bar{y}/H \ , \quad t = \dot{\gamma}_o \bar{t} \ , \quad s = \bar{s}/\kappa \ , \quad v = \bar{v}/H\dot{\gamma}_o \ , \quad \theta = \bar{\rho}c\bar{\theta}/\kappa \\ &\rho = \bar{\rho} H^2 \dot{\gamma}_o^{\,2}/\kappa \ , \quad k = \bar{k}/\bar{\rho}cH^2\dot{\gamma}_o \ , \quad a = \kappa\bar{a}/\bar{\rho}c \ , \quad b = \dot{\gamma}_o \bar{b} \end{aligned} \tag{3}$$

Here H is the slab half thickness, $\dot{\gamma}_o$ is the average applied strain rate, κ is the isothermal slow flow stress, and c is the heat capacity.

Since the material has been assumed to be rigid/plastic, there is no elastic component of deformation, and the velocity gradient is equal to the plastic strain rate. In (2.2) the term $sv_{,y}$ represents plastic work, which is assumed to be converted completely to heat. Equation (2.3) is simply an assumed flow law which exhibits the properties of thermal softening and rate hardening, and which also has a nonzero yield stress when the strain rate vanishes. Boundary conditions are $v(\pm 1,t) = \pm 1$ and $\theta_{,y}(\pm 1,t) = 0$. Initial conditions are $\theta(y,0) = \theta_o(y)$ prescribed, with compatible values for $v_{,y}$ and s = constant determined from the formulas

$$v_{,y} = \frac{1}{b}\left[\left(\frac{s}{1 - a\theta}\right)^{1/m} - 1\right] \ , \quad s = (1 + b)^m \left[\int_o^1 \frac{dy}{(1 - a\theta)^{1/m}}\right]^{-m} .$$

The first follows from the flow law (2.3), and the second follows by integrating the first and taking account of the boundary condition on v.

When $\theta_o(y) = 0$ identically, equations (2) have the following simple homogeneous solutions,

$$v = y \ , \quad s = \frac{\Gamma}{a} e^{-\Gamma t} \ , \quad \theta = \frac{1}{a}(1 - e^{-\Gamma t}) \ , \tag{4}$$

where $\Gamma = a(1 + b)^m$. This solution is shown in Figure 2. At the initial time, when the motion is started and the temperature is zero everywhere, the stress jumps up due to the rate effect. Thereafter, it decays exponentially toward zero, and the temperature grows exponentially toward 1/a.

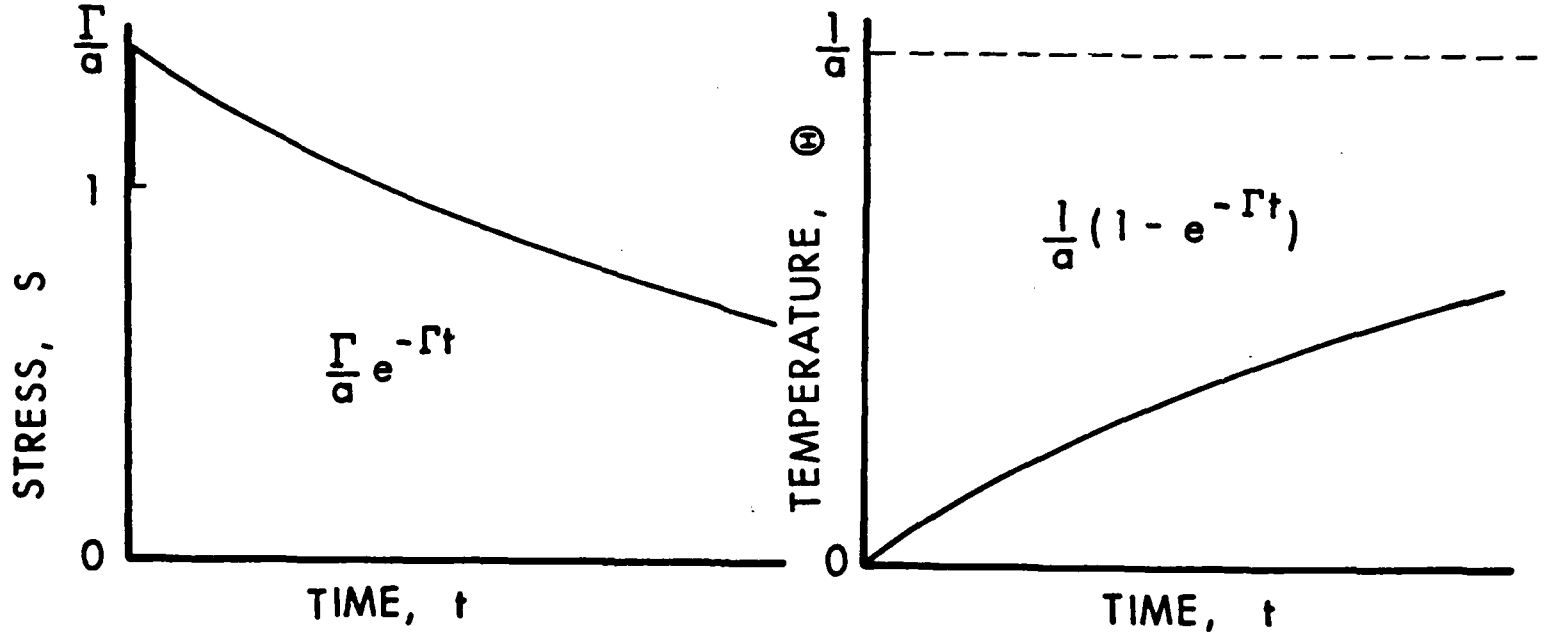

Figure 2. The evolution of stress and temperature for the simplified model in the homogeneous case, where $v_{,y} = 1$ throughout.

Since the average or nominal strain rate in nondimensional terms is 1, nondimensional time and strain are numerically equal, so the material strain softens right from the start. It is this softening that presents the opportunity for localization.

Of far greater interest than the simple homogeneous solution are problems where the initial conditions are not quite uniform. In the next two sections the initial temperature will be assumed to be symmetric in y and given by

$$\theta_o(y) = \varepsilon\psi_o(y), \quad \text{where} \int_o^1 \psi_o(y)dy = 1 \tag{5}$$

That is to say, the initial temperature is nearly zero (i.e., equal to the reference temperature), and its average defines a small positive parameter ε. Furthermore, temperature and stress will be symmetric and velocity antisymmetric in y at all times, so the problem, including the boundary conditions, is redefined in the obvious way on the interval $0 \leq y \leq 1$.

3. NUMERICAL SOLUTIONS

Previous numerical solutions, Wright and Batra,[7 8 9] were subject to numerical instability as localization became extreme, so a modified approach was taken here. First the equations were cast into weak form and discretized spatially by a symmetric Galerkin method, as previously, but now the grid was divided into equal segments on a logarithmic scale, so as to crowd a large number of nodes into the center of the band, where the appropriate number was found by trial and error. Piecewise linear global basis functions were used to interpolate the velocity and temperature fields (the fundamental unknowns) as well as the corresponding test functions. After performing the required integrations, the equations have the form

$$M\dot{u} = f(u)$$

where M is a combined mass/heat capacity matrix and u is the vector of nodal velocities and temperatures. Since the matrix M is positive definite, banded, and diagonally dominant, its inverse is strongly diagonally dominant, so that, after multiplying through by M^{-1}, a banded approximation of the Jacobian of the new right hand side may be used. This fact is useful in reducing storage requirements and evaluation time for the Jacobian matrix. The problem has now been reduced to an initial value problem for a finite system of coupled nonlinear ordinary differential equations. The boundary conditions, of course, are implied by the weak form of the equations together with the correct choice of test functions. Time integration was performed by the method of lines, that is, simply using one of the many efficient algorithms in existence for the solution of systems of ODE's. The one used here was Gear's stiff method,[12] as implemented in the standard IMSL FORTRAN library.[13]

For the initial conditions $\theta_o(y) = 0.1\ (1 - y^2)^9\ e^{-5y^2}$, typical results are illustrated in Figures 3-5, which show the solution surfaces

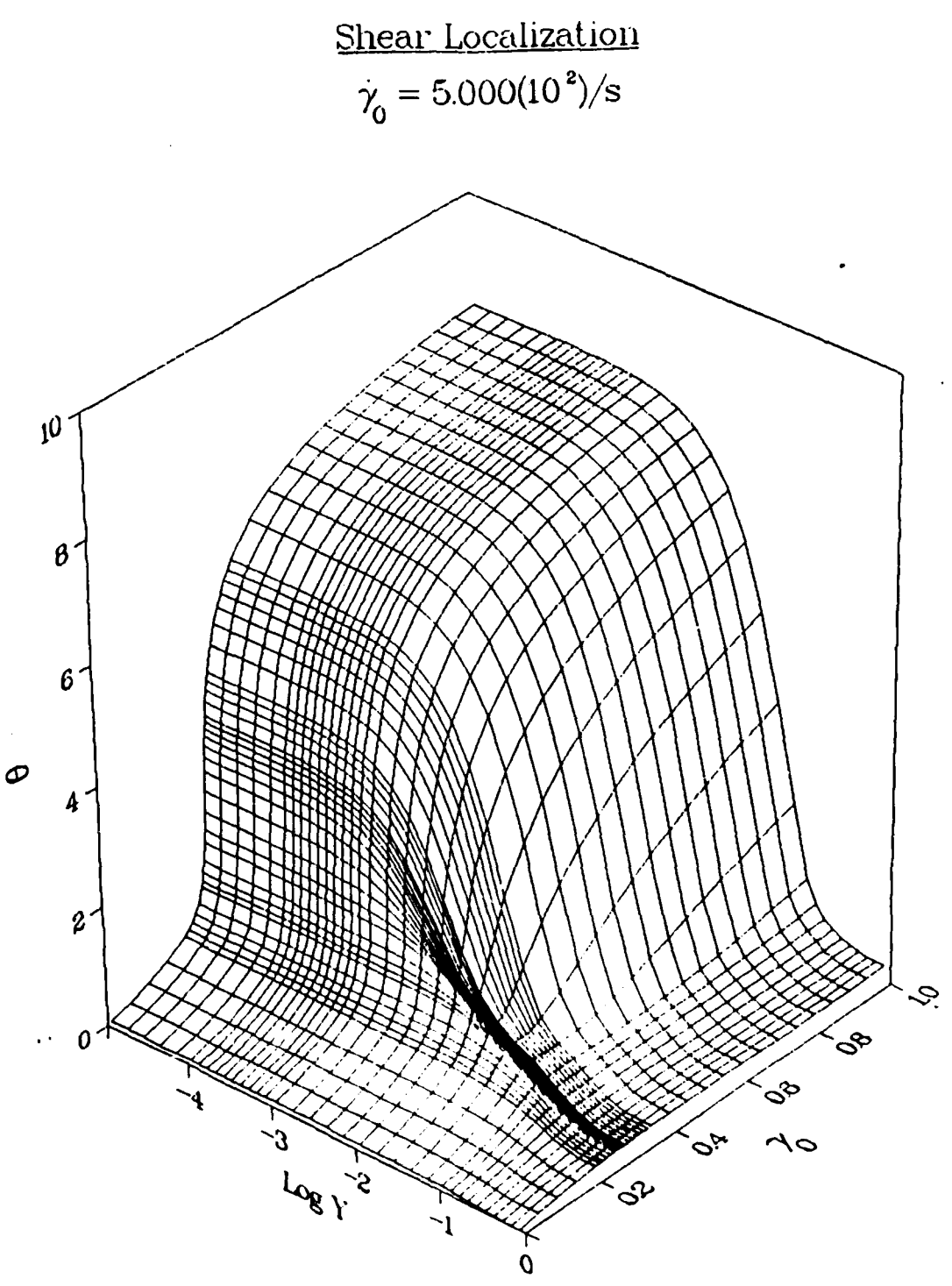

Figure 3. Solution surface for temperature as a function of position and nominal strain (time). The logarithmic scale in y is used to resolve the severe localization.

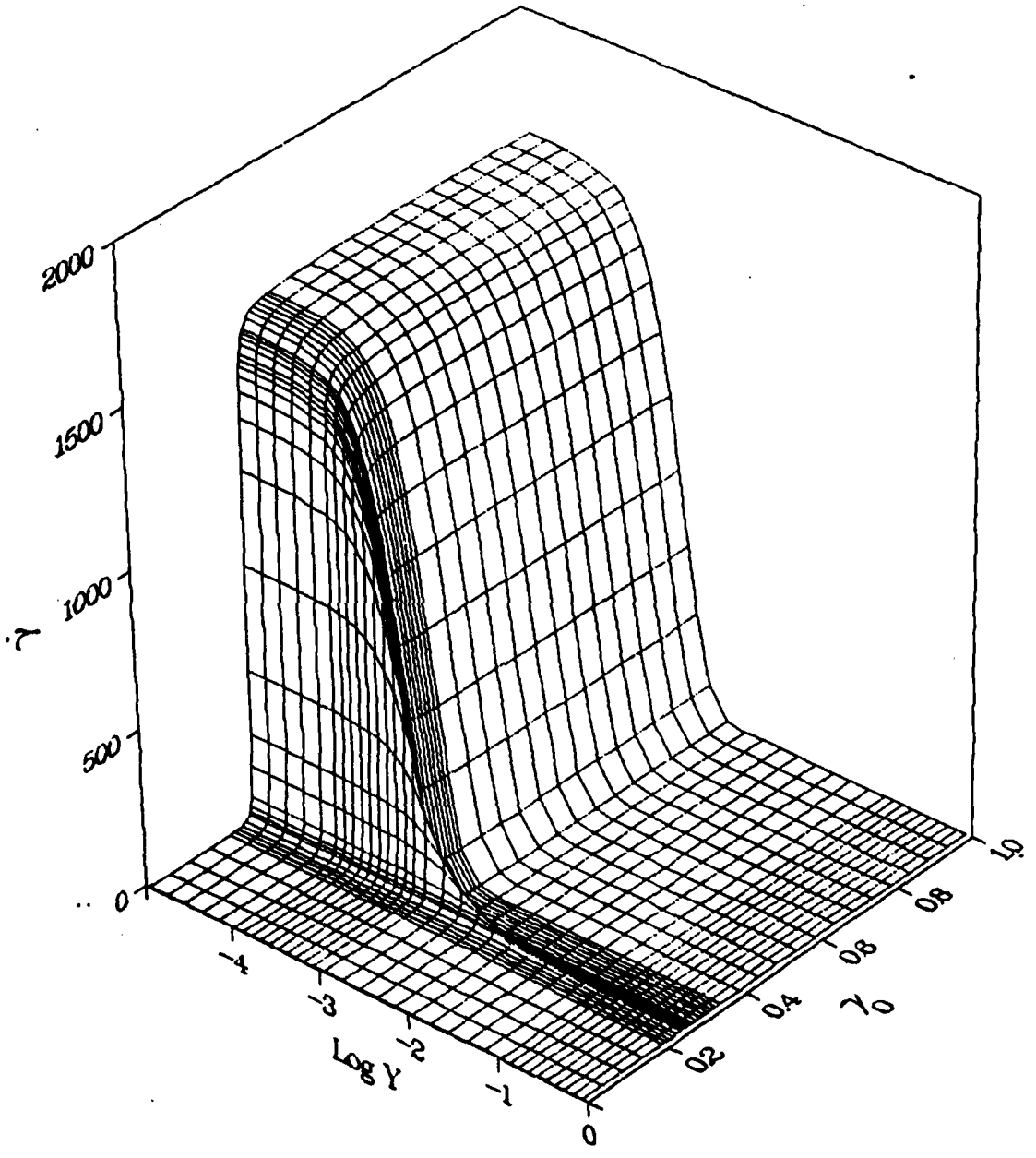

Figure 4. Solution surface for strain rate as a function of position and nominal strain (time). The logarithmic scale in y is used to resolve the severe localization.

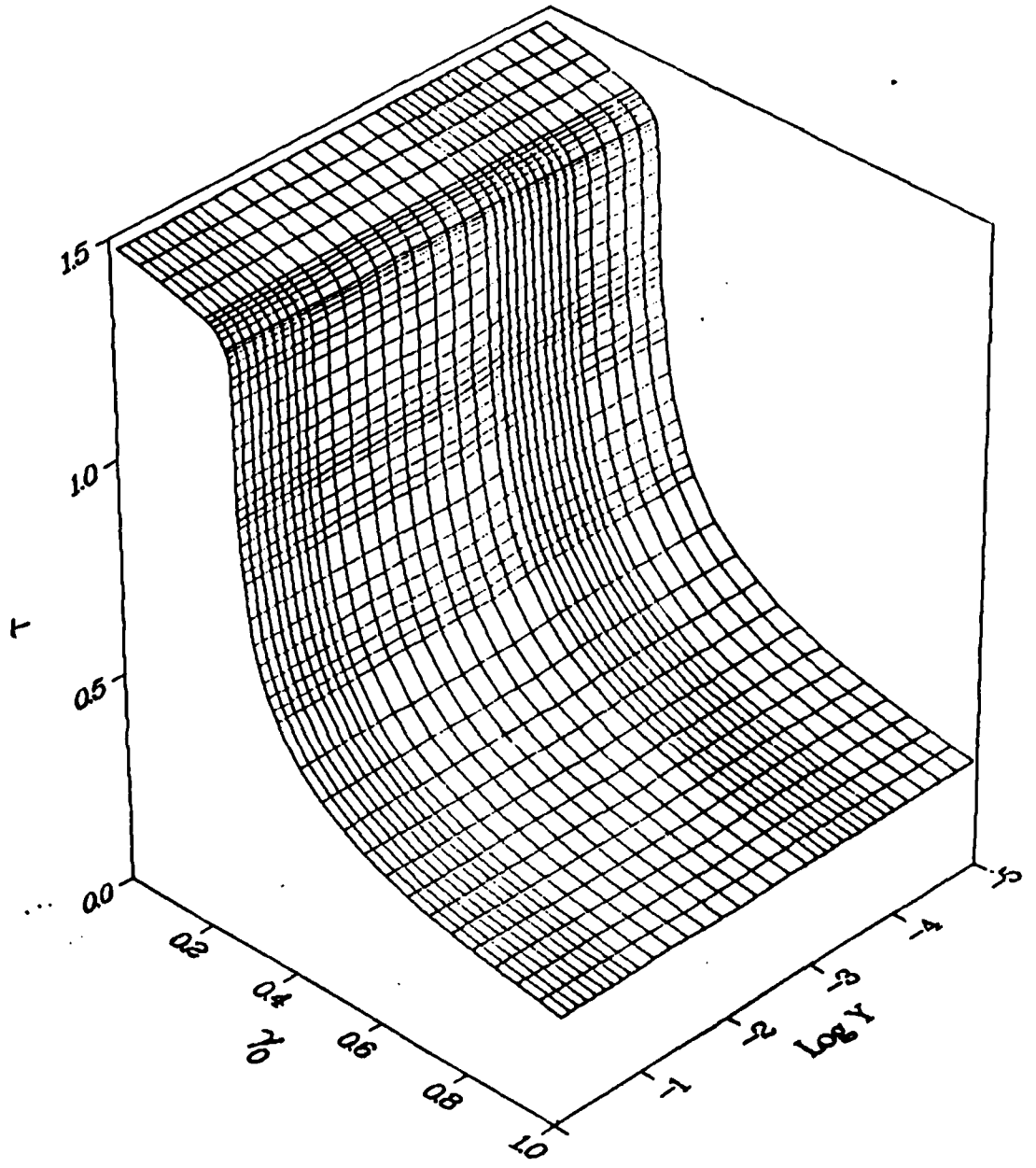

Figure 5. Solution surface for stress as a function of position and nominal strain (time). Stress is very uniform in y.

for temperature, plastic strain rate, and stress for a nominal strain rate of $\dot{\gamma}_o = 500\ s^{-1}$. The nondimensional parameters in (3) were taken to be $\rho = 3.93 \times 10^{-5}$, $k = 0.0022$, $a = 0.104$, $m = 0.0251$, and $b = 5 \times 10^6$ for this calculation. On the scale shown, the initial perturbation is scarcely visible, and although the perturbation grows right from the start, severe localization is considerably delayed, and the stress follows nearly the same early history as if there were no perturbation at all. Eventually severe localization does occur with the temperature increasing sharply in the center of the band, the plastic strain rate rising nearly instantaneously in the center, and the stress falling markedly. At the edges of the band the plastic strain rate falls to zero and the temperature becomes essentially constant, although at very long times the edge temperature will rise some more due to the insulated boundary and heat conduction from the center. After the rapid transition period, the temperature continues to rise in the center and the stress continues to fall, but at a much reduced rate. However, the plastic strain rate reaches a saturation profile and becomes completely independent of time. Note also that the stress is nearly constant in y at all times.

Other runs have been made at nominal strain rates of 5, 50, 5000, and 50000 s^{-1}, but with the same initial conditions as previously. At these rates the nondimensional parameters change from their previous values according to the scalings given by (3), and in each case the results remain qualitatively the same, but with some significant differences, which are summarized in Figures 6-8. At the lower rates Figure 6 shows that thermal diffusion broadens and softens the rapid transition region, as measured by the rise time for transition. Figure 7 shows that as the rate increases the saturation profile becomes much narrower and taller. These results were computed for particular initial conditions, but the saturation profile actually is completely independent of the initial conditions and depends only on the nominal strain rate. This will be demonstrated analytically in a later section. Figure 8 shows the critical strain for extreme localization. Although the patterns shown in the previous two figures may not seem too surprising, Figure 8 does not follow readily in any obvious way. Finally, at the highest rates, the stress profile is no longer nearly uniform in y for all times, but during the rapid transition, it drops first in the center and later at the outside. This is a wave propagation effect due to the fact that the nondimensional density scales as the square of the applied strain rate in (3). At the highest rate the density has become comparable to 1 so the inertia term is no longer insignificant.

4. REGULAR PERTURBATION SOLUTIONS AT EARLY TIMES

The early growth of a small nonuniformity can be easily understood by means of a regular perturbation analysis, where the perturbation is taken with respect to the homogeneous solution in (4). That is, the response functions s, θ, v will be written as

$$s = s_H + \varepsilon\tilde{s} + \ldots \quad , \quad \theta = \theta_H + \varepsilon\tilde{\theta} + \ldots \quad , \quad v = v_H + \varepsilon\tilde{v} + \ldots \qquad (6)$$

where the subscript H refers to the homogeneous solution (4), and ε is a small parameter defined by the initial temperature distribution as in (5).

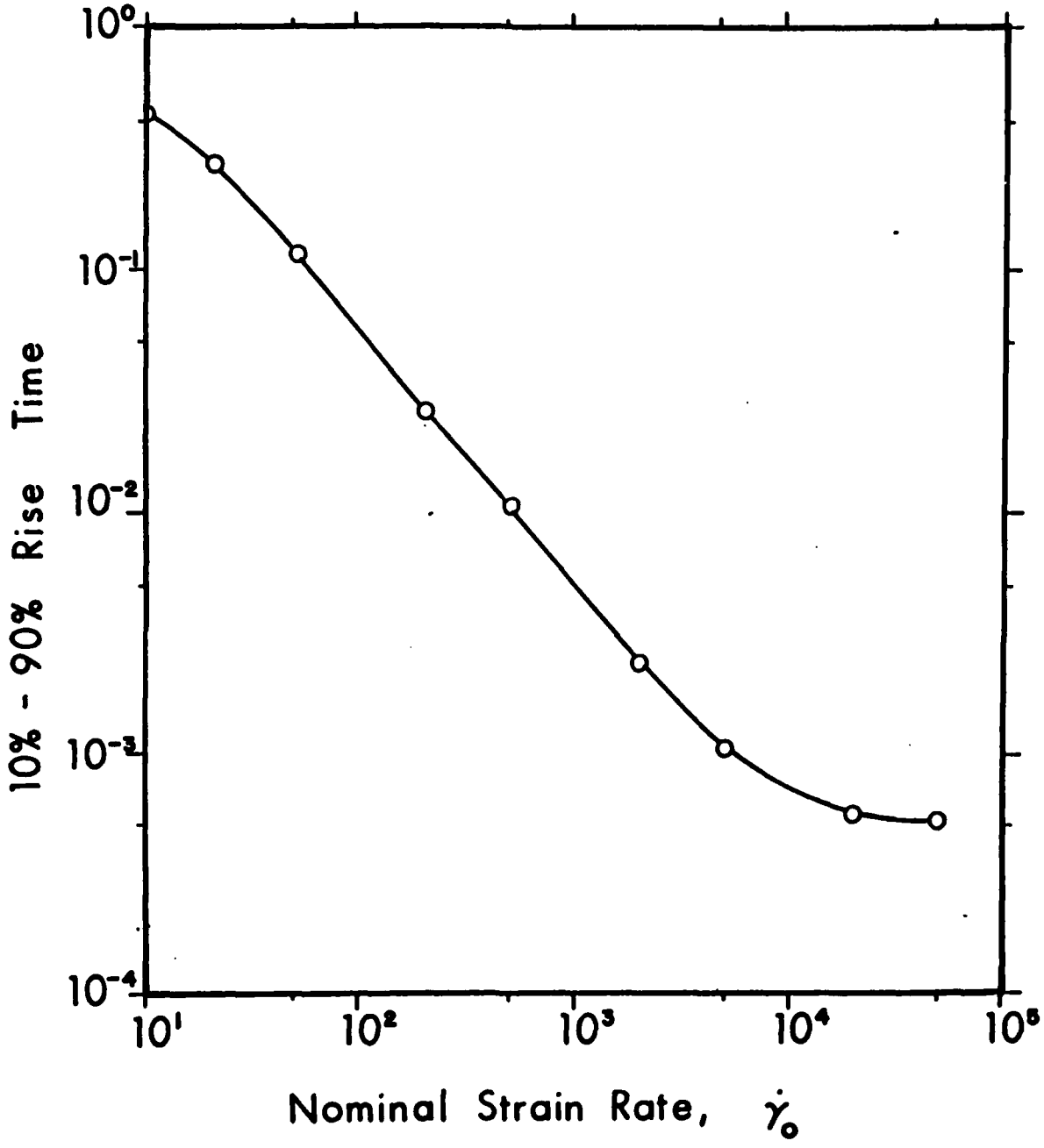

Figure 6. Rise time vs. nominal strain rate. Nondimensional thermal diffusivity decreases as strain rate increases and causes a shorter rise time.

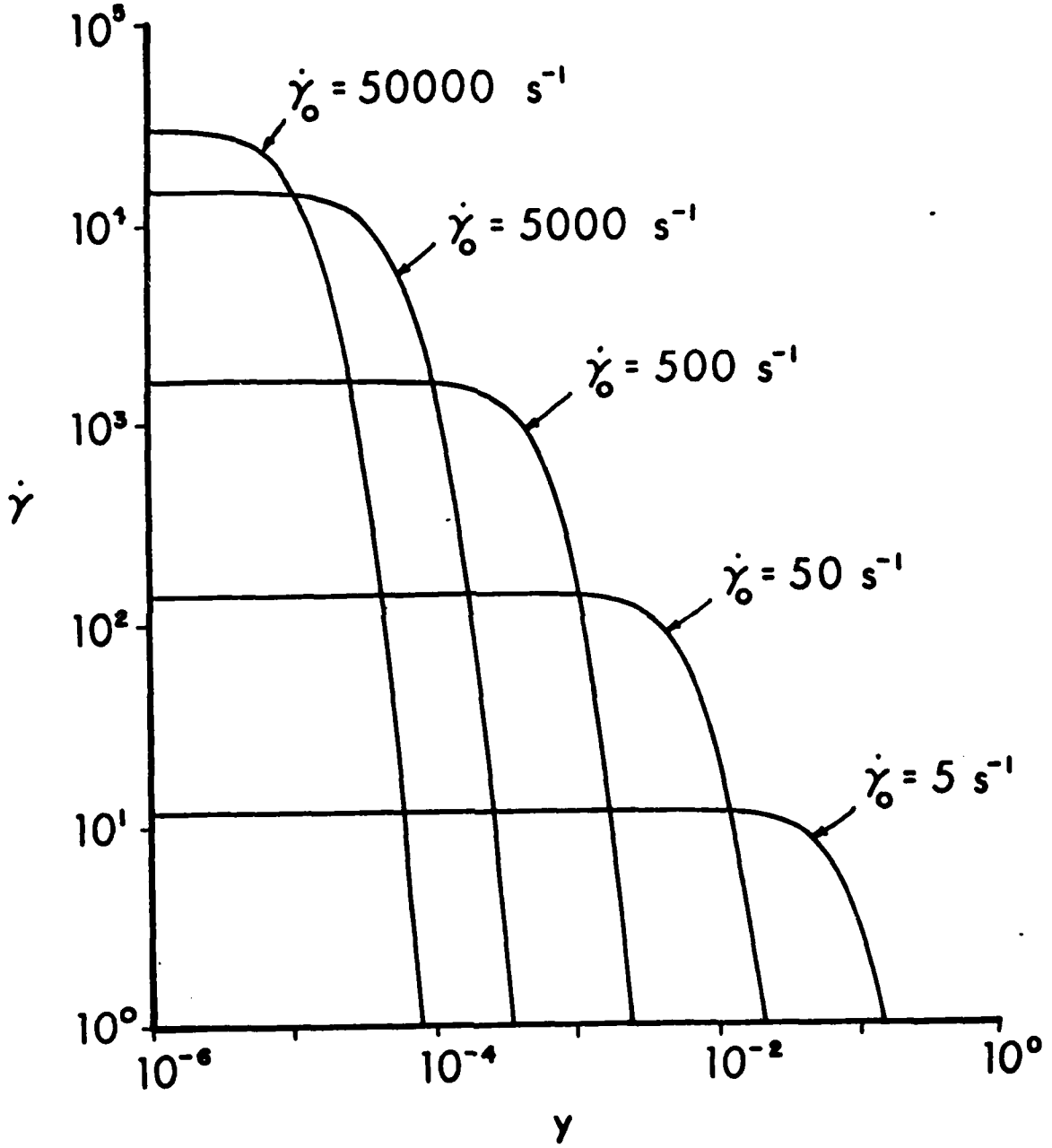

Figure 7. Saturation profile (late times) of strain rate vs. position. The logarithmic scale is needed to resolve the severe localization.

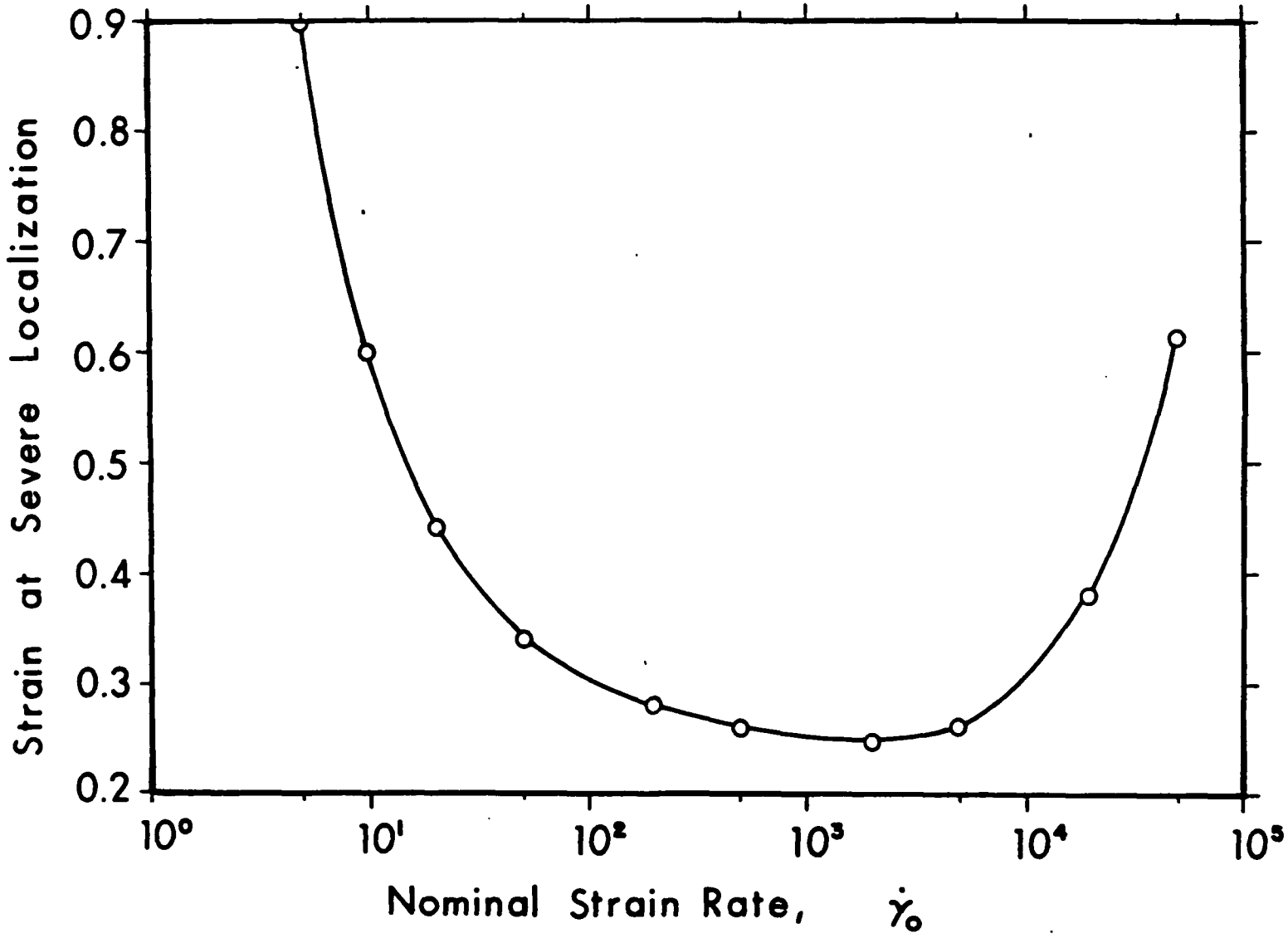

Figure 8. Critical strain for severe localization as a function of nominal strain rate.

Advantage will also be taken of the numerical result that the stress is uniform in y to a high degree of approximation unless the nominal strain rate is very large. The equations of first variation (written without the tildes) become

$$s_{,y} = 0$$

$$v_{,y} = \frac{a}{\bar{m}\Gamma} e^{\Gamma t} s + \frac{a}{\bar{m}} e^{\Gamma t}\theta \tag{7}$$

$$\theta_{,t} = k\theta_{,yy} + \frac{1 + \bar{m}}{\bar{m}} s + \frac{\Gamma}{\bar{m}} \theta$$

$$\text{where } \bar{m} = m \frac{b}{1 + b} .$$

Clearly these equations lose validity for large times, but here the interest is only in small times. Boundary and initial conditions are given by

$$\text{B.C.;}\quad v(0,t) = v(1,t) = 0 \text{ and } \theta_{,y}(0,t) = \theta_{,y}(1,t) = 0.$$

$$\text{I.C.;}\quad \theta(y,0) = \psi_o(y)$$

with initial values for $v_{,y}$ and s compatible through use of (7.2) above and (8) below. From (7.1) $s = S(t)$, and by integrating (7.2) we have

$$S(t) = -\Gamma\int_o^1 \theta(y,t)\, dy. \tag{8}$$

With this result in (7.3) and by integrating again we have

$$\frac{d}{dt}\int_o^1 \theta(y,t)dy = -\Gamma\int_o^1 \theta(y,t)dy.$$

Thus the perturbation in stress is related to the perturbation in mean temperature by (8) and is given by

$$S(t) = -\Gamma\, e^{-\Gamma t}. \tag{9}$$

Equation (7.3) now becomes

$$\theta_{,t} = k\theta_{,yy} + \frac{\Gamma}{\bar{m}}\theta - \Gamma\frac{1 + \bar{m}}{\bar{m}} e^{-\Gamma t}. \tag{10}$$

With the decomposition $\theta = e^{\Gamma t/\bar{m}} \left\{\psi(y,t) + \phi(t)\right\}$, (10) may be split into two simpler equations,

$$\psi_{,t} = k\psi_{,yy} \quad \text{and} \quad \phi_{,t} = -\Gamma\frac{1 + \bar{m}}{\bar{m}} e^{-\Gamma\frac{1 + \bar{m}}{\bar{m}}t}. \tag{11}$$

The appropriate choices for initial conditions are $\psi(y,0) = \psi_o(y)$ and $\phi(0) = 0$, and the boundary conditions for ψ are $\psi_{,y}(0,t) = \psi_{,y}(1,t) = 0$. The final result is a solution of (2), which is exact to first order in ε.

$$s = \frac{\Gamma}{a}(1 - a\varepsilon)\, e^{-\Gamma t} + O(\varepsilon^2)$$

$$\theta = \frac{1}{a}\left[1 - (1 - a\varepsilon)e^{-\Gamma t}\right] + \varepsilon e^{\frac{\Gamma}{\bar{m}}t}\,(\psi - 1) + O(\varepsilon^2) \qquad (12)$$

$$v_{,y} = 1 + \varepsilon \frac{a}{\bar{m}}\, e^{\frac{\Gamma}{\bar{m}}t}\,(\psi - 1) + O(\varepsilon^2)$$

The perturbation and finite element solutions are compared in Figure 9a-9e, which show the temperature, plastic strain rate, and stress near the center of the band, as computed by the two methods. Initially the results coincide because of the choice of initial conditions, of course. In the example shown, $\varepsilon = 0.02327$, and the perturbation solution remains reasonably close to the finite element solution until $\gamma_p = 0.15$ or so (for other values of y the two solutions are even closer), but eventually the two diverge widely.

Note that the first term in each expression in (12) describes the behavior of the spatial mean for that field variable, and that it behaves exactly as the homogeneous solution would if the initial temperature were ε rather than 0. The function ψ has a spatial mean of 1 for all time and evolves from its initial values toward the constant value of 1 according to simple heat diffusion in a slab with insulated boundaries. The variations from the mean of temperature and strain rate depend on $\psi - 1$ with a simple exponential amplification, but the stress to order ε is completely unaffected by the nonuniformity in the other field variables. The very striking result is that although the simple perturbation approach, previously used by many other workers in considering stability of similar problems (e.g., Clifton,[3] Burns,[6] Bai,[5] predicts the correct initial growth of perturbations after peak homogeneous stress, it completely fails to predict anything at all about the later explosive growth in temperature and plastic strain rate and the simultaneous collapse of the stress.

Results so far may be summarized as follows. Numerical computation shows that band formation is a multi-stage process. In the first stage, described by the simple perturbation analysis, there is slow growth only. (When the rapid change occurs, the term $\varepsilon e^{\Gamma t/\bar{m}}$ is still much less than one.) Subsequently there is an extremely rapid transition, during which almost all of the localization occurs, followed by a late, quasi-steady stage, which will be described in a later section.

5. AN ABSOLUTE STABILITY CRITERION

Although no perturbation analysis to date sheds any light on the timing and structure of the rapid transition, the simple analysis does give an absolute stability criterion that determines conditions under which perturbations decay right from the start. In (12.2) and (12.3) growth occurs

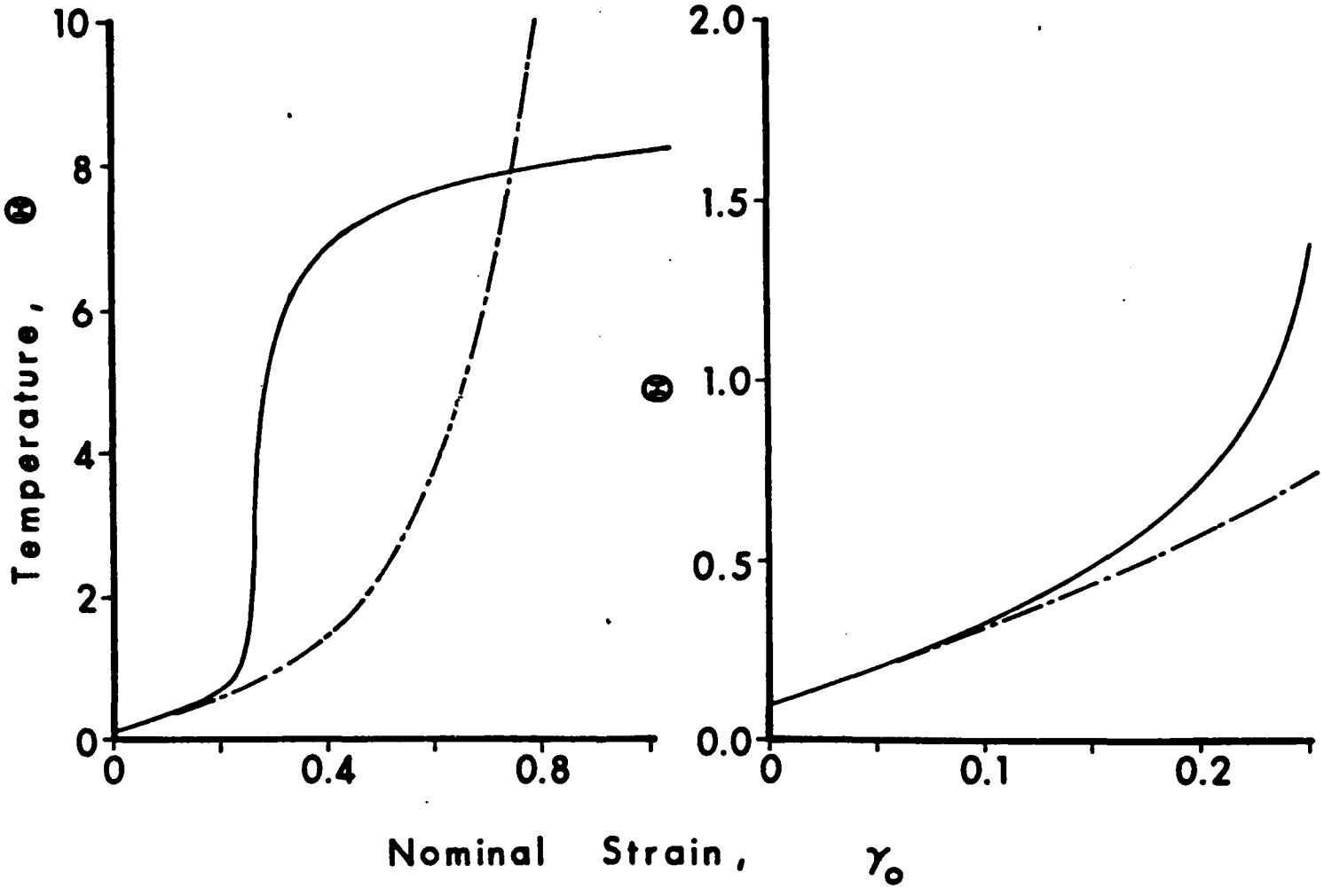

Figure 9a. Maximum temperature vs. nominal strain (time). The numerical and perturbation solutions are shown by the solid and interrupted lines respectively. 9b. Same as 9a., but with expanded scales.

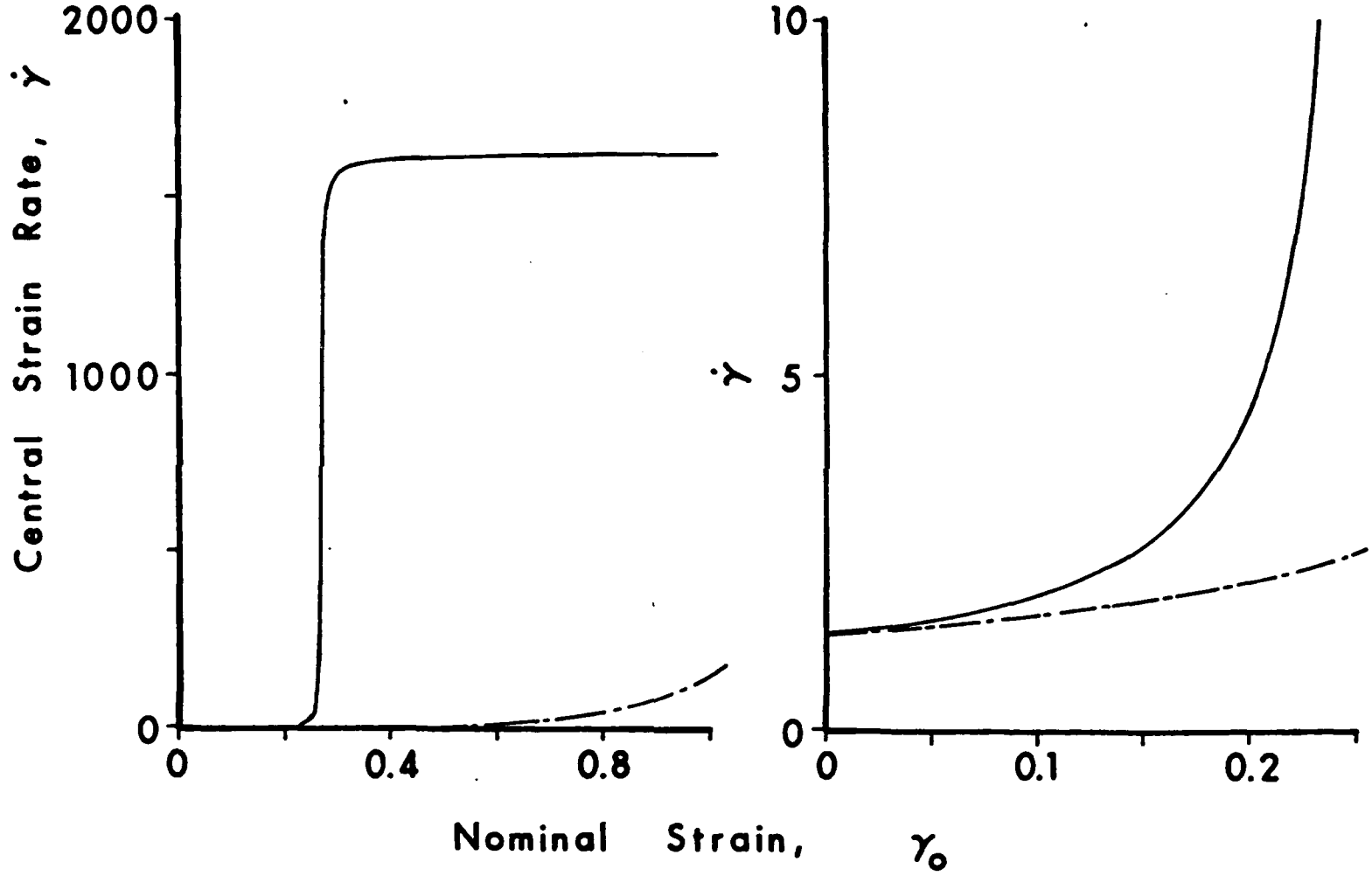

Figure 9c. Maximum strain rate vs. nominal strain (time). The numerical and perturbation solutions are shown by the solid and interrupted lines respectively. 9d. Same as 9c., but with expanded scales.

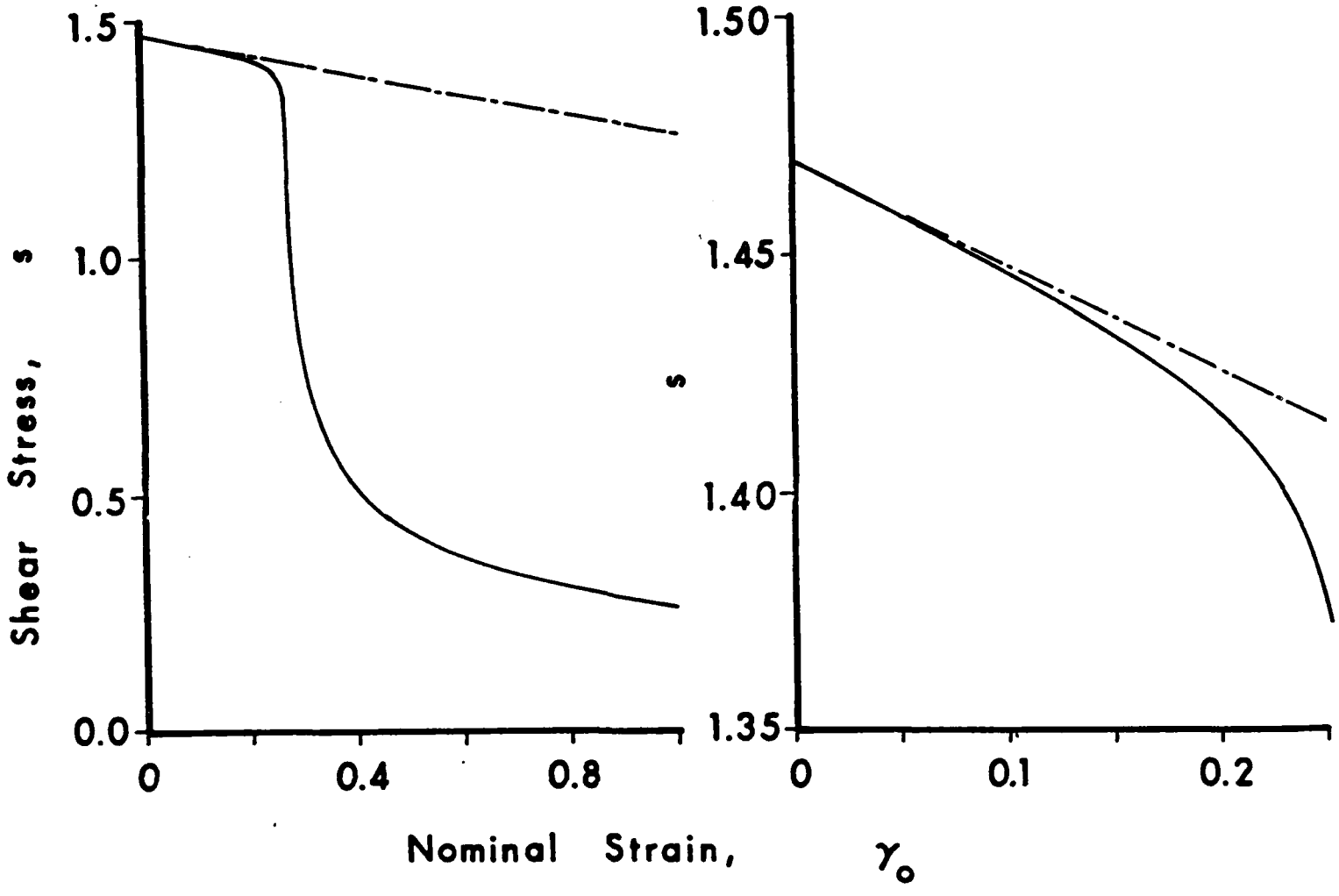

Figure 9e. Shear stress vs. nominal strain (time). The numerical and perturbation solutions are shown by the solid and interrupted lines respectively.
9f. Same as 9e., but with expanded scales.

because of the positive exponential term, but if heat production from plastic work is not too strong relative to heat conduction, then no growth will occur, even though stress decreases with strain. This may be seen by considering the Fourier components of $\psi - 1$ in (12),

$$\psi - 1 = \sum_{n=1}^{\infty} a_n e^{\alpha_n t} \cos n\pi y, \qquad \text{where} \quad \alpha_n = -(n\pi)^2 k.$$

This expression satisfies (11.1), together with its boundary conditions, and the coefficients a_n are to be chosen so as to match the initial conditions. Clearly the nth components of θ and $v_{,y}$ in (12) will decay provided

$$\frac{\Gamma}{\bar{m}} < k\, n^2 \pi^2.$$

In dimensional terms, the criterion for decay of the nth Fourier component is

$$\kappa \bar{a} H^2 \,(1 + \bar{b}\dot{\gamma}_o)^{1+m} \quad < \bar{m} k \bar{b} (n\pi)^2, \tag{13}$$

Thus, all Fourier components above a certain threshold decay; increases in strength, thermal softening, slab thickness, or nominal strain rate all tend to be destabilizing; and an increase in thermal conductivity tends to be stabilizing. The influence of the two parameters m and b for rate hardening is not quite so readily apparent, since each appears on both sides of the inequality. It turns out that increases in either parameter may be stabilizing or destabilizing depending on relative values of $\bar{b}\dot{\gamma}_o$ and m. To see this, suppose that equality holds in (13), and by differentiating, determine which way the inequality will turn for small increases in $\bar{b}$ or m. The results are as follows.

If equality holds in (13), then with all other quantities held constant,

$$\begin{aligned} &\text{an increase in } \bar{b} \text{ is stabilizing if} \quad \bar{b}\dot{\gamma}_o < \frac{1}{m} \quad , \text{ and} \\ &\text{an increase in m is stabilizing if} \quad \ln(1 + \bar{b}\dot{\gamma}_o) < \frac{1}{m} \quad . \end{aligned} \tag{14}$$

If the inequalities in (14) are reversed, then increases are destabilizing. For the numerical values used in this paper, an increase in m is stabilizing, but surprisingly enough, an increase in $\bar{b}$ is destabilizing.

With n = 1 the inequality (13) gives an absolute stability criterion which may be used to find the threshold value of $\dot{\gamma}_o$ below which all Fourier components decay. In this paper the threshold is 2.06 s^{-1}, which has been confirmed numerically by running cases just below and just above this value. At 2.05 s^{-1} the temperature distribution eventually becomes essentially uniform and the plastic strain rate becomes nearly 1 everywhere. At 2.075 s^{-1} a steady, but nonuniform, profile of plastic strain rate eventually forms at large times.

6. LATE STAGE MORPHOLOGY

As remarked previously, the numerical results indicate that after the rapid transition to a completely localized deformation pattern, the plastic strain rate seems to be independent of time. Therefore, let it be assumed that $v_{,y} = p(y)$, and since v is constant on the boundaries, we have $v_{,t} = 0$ and $s_{,y} = 0$. Thus it follows from the flow law (2.3) that the temperature may be written in the separable form

$$(1 - a\theta) = S(t)\, h(y) \tag{15}$$

where $s = S(t)$ and $h(y) = 1/[1 + bp(y)]^m$, or for other rate factors $f(v_{,y})$ in the flow law, $h(y) = 1/f(p)$. With (15) substituted into the energy equation (2.2), then after dividing through by $S(t)h(y)$ and using the usual separation argument, independent equations for S(t) and h(y) are derived.

$$\begin{aligned} S_{,t} + \alpha S &= 0 \\ kh_{,yy} + \alpha h &= af^{-1}\left(\frac{1}{h}\right) \end{aligned} \tag{16}$$

where α is a separation constant, and for the rate factor used in this paper $f^{-1}(1/h) = b^{-1}(h^{-1/m} - 1)$. The solution to (16.1) is

$$S = S_o e^{-\alpha(t-t_o)} \tag{17}$$

where S_o is the stress level at $t = t_o$, and a first integral to (16.2) may be written

$$h_{,y}^2 = \frac{2}{k}\int_{h(o)}^{h} [af^{-1}(1/h) - \alpha h]\, dh = F(h;h(0),\alpha), \tag{18}$$

where the function F is defined by (18), and the parametric dependence of F on h(0) and α is indicated explicitly. At $y = 0$, $h = h(0)$, so the condition $h_{,y}(0) = 0$ is satisfied (vanishing temperature gradient in the center of the band due to symmetry). After taking the positive square root in (18), the solution for h follows by quadrature, but it is still necessary to determine the parmeters α and h(0). These must be chosen so as to meet the required boundary conditions at $y = 1$, which in effect defines a nonlinear eigenvalue problem. The required conditions are

$$h_{,y}(1) = 0, \text{ and } v(1) = 1.$$

In terms of the function F, these may be written

$$\begin{aligned} &F(h(1);h(0),\alpha) = 0 \\ &\int_o^1 v_{,y}\, dy = \int_{h(o)}^{h(1)} \frac{f^{-1}(1/h)\, dh}{\sqrt{F(h)}} = 1 \end{aligned} \tag{19}$$

In addition, to ensure that h(y), as determined by the quadrature, actually takes on the value h(1) when y = 1, it is necessary to have

$$\int_0^1 dy = \int_{h(o)}^{h(1)} \frac{dh}{\sqrt{F(h)}} = 1 \tag{20}$$

Equations (19.1), (19.2), and (20) are to be solved for h(0), h(1), and α. It does not seem possible to state unequivocally that these three equations always have a solution, but when they do, as numerical experience to date has always indicated, integration of (18) yields y as a function of h. It usually happens that an unloading boundary appears somewhere in the problem where h = 1 and $f^{-1}(1/h) = v_{,y} = 0$. Since f is only defined for $v_{,y} \geq 0$ and only takes on values of 1 or greater, $f^{-1}(1/h)$ is directly defined only for $0 \leq h \leq 1$. However, the unloading cases can be included without modification in the preceding framework simply by extending the function f^{-1} to be defined by $f^{-1}(1/h) = 0$ if $h > 1$. The net result is that for fixed values of the nondimensional parameters ρ, k, a, b, and m, there is a definite quasi-steady end state with a fixed distribution of plastic strain rate. In particular, the end state is absolutely independent of the initial conditions. This result has also been amply demonstrated by numerical experimentation.

The quasi-steady result above may seem somewhat special because the separation property required to obtain (16) depends entirely on the linear dependence of stress on temperature in the assumed flow law (2.3). There is strong evidence, however, that a similar, if slightly weaker, result will hold in more general cases. If $v_{,t}$ and $\theta_{,t}$ are set equal to zero in (2.1) and (2.2), then solutions to the resulting equations are steady solutions for the full set. Properties of such steady solutions have been described in a recent paper.[11] In general, there is a two parameter family of solutions which meet the required boundary conditions at y = 0, but which cannot be made to meet the boundary conditions at y = 1 except in very unusual circumstances. (This is in contrast to the quasi-steady solutions above which do meet all required boundary conditions.) The steady solutions would then seem to represent the center of the fully developed shear bend as a boundary layer where the two defining paramters may be "slowly varying" in some sense. In a more general case than considered here, suppose the flow law is $s = g(\theta, v_{,y})$ where g increases monotonically with $v_{,y}$. Then the plastic strain rate may be written $v_{,y} = p(\theta;s)$, where s is constant in a steady solution, and the temperature and velocity distributions are found from

$$\begin{aligned} \frac{1}{2}k\theta_{,y}^2 &= s\int_0^{\theta_c} p(\theta;s)\, d\theta \\ v &= \sqrt{\frac{2k}{s}} \left\{ \int_0^{\theta_c} p(\theta;s)\, d\theta \right\}^{1/2} \end{aligned} \tag{21}$$

In (21.1) θ_c is the temperature in the center of the band, and the negative square root is to be taken to find $\theta_{,y}$. The two parameters in (21) that explicitly define which solution is to be considered are s and θ_c, but these could be expressed in terms of many other parameters, such as the plastic strain rate in the center of the band or the limiting values of v and $\theta_{,y}$ given by (21) at large values of y. Figure 10 shows how well the solution given by (21) matches the numerical solution when the temperature and plastic strain rate in the center of the band, as found numerically, are used as the defining parameters. Such excellent agreement in the core of the band is only possible after the rapid transition region, of course.

7. NUMERICAL EXPERIMENTS ON TDHE TIME OF STRESS COLLAPSE

Analysis has given very satisfactory descriptions of the early and late time morphology of a shear band, but has not yet given an adequate description of either the timing or the structure of the transition between the two. Consequently, a series of numerical runs was made in which the magnitude and shape of the initial temperature distribution were varied in a simple way, and the time to severe localization was computed. All these calculations were made for a nominal strain rate of $\dot{\gamma}_o = 500\ s^{-1}$. The initial temperature distribution was taken to be triangular with a peak temperature at y = 0, where $0 < \theta_o(0) < 1/a$. The temperature decreased linearly in y with negative slope K, and reached 0 at a value of y between 0 and 1. The magnitude of the perturbation is then measured by the area of the triangle ε, as in the linearized perturbation analysis, and the shape is measured by the slope K, a small value of K indicating a flat, spread out shaped and a high value indicating a sharply peaked shape.

Figure 11 shows the nominal strain achieved at severe localization as a function of ε when K is held constant, and Figure 12 shows the strain at severe localizataion as a function of K when ε is held constant. The two solid dots on the curves in Figure 11 correspond to the two solid dots in Figure 12. Although these curves certainly do not give the whole variation in response as magnitude and shape are varied, they are highly suggestive. At small magnitudes in Figure 11 the localization strain varies slowly at a low negative power of amplitude and is independent of the value of K. However, for the larger ε, the strain decreases rapidly over several orders of magnitude for relatively modest changes in ε if the slope is large, but changes scarcely at all if the slope is small. On the other hand, Figure 12 shows that the strain to localization is a relatively weak function of shape for small amplitudes, but Figure 11 indicates that it must be a far stronger function of shape for larger amplitudes. When the initial shape is very flat and K is small, Figure 12 shows that the strain at severe localization appears to approach a function that decreases linearly with the logarithm of slope, which would indicate that the strain tends to infinity as the slope tends to zero. That is to say, a perfectly flat or constant initial temperature distribution does not localize. For larger values of K, where the profile is sharply peaked in the center, heat conduction and inertia very rapidly smooth out the distribution to make it

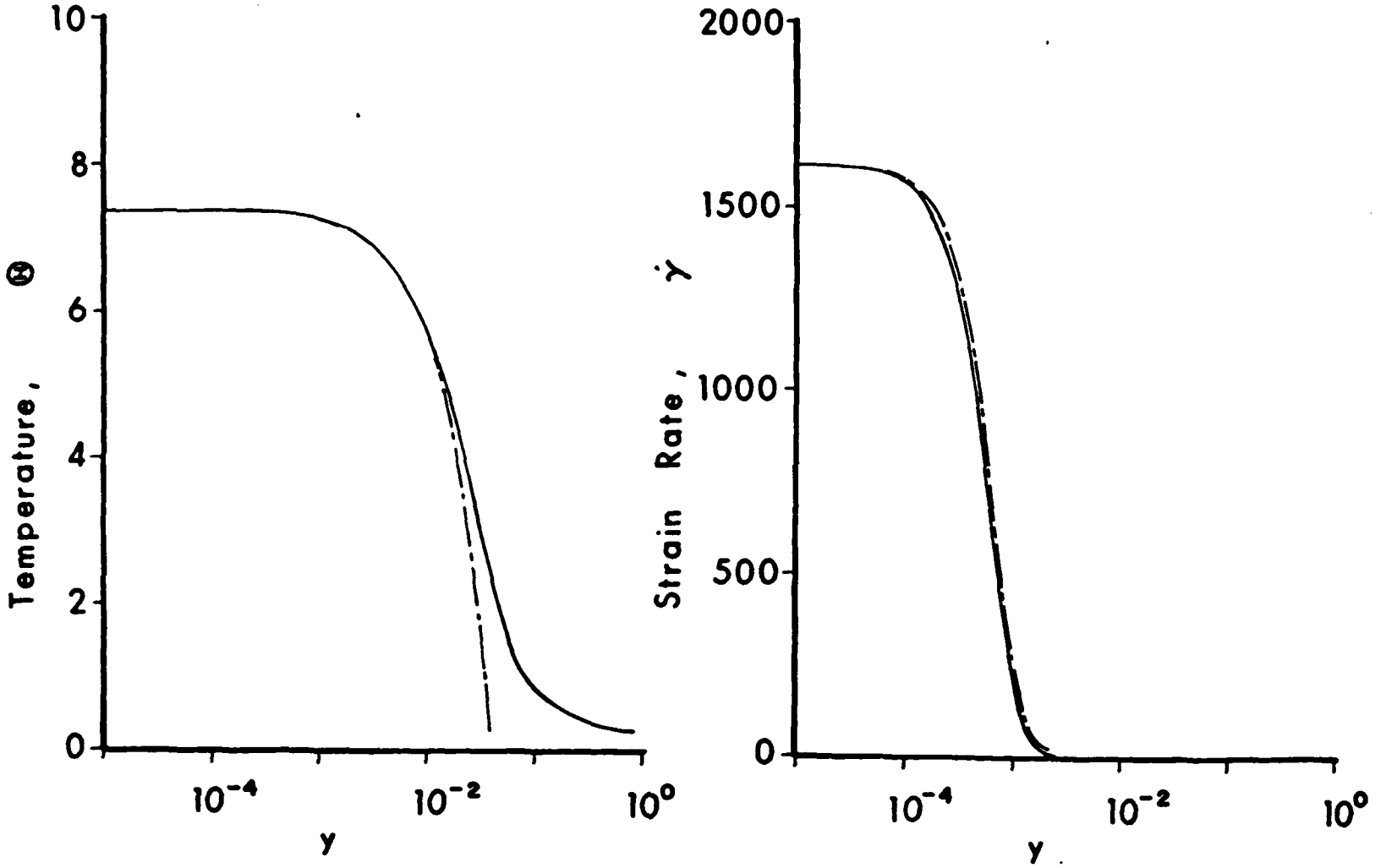

Figure 10. Saturation (late time) profile of temperature and strain rate at a nominal rate of $\dot{\gamma}_0 = 500\ s^{-1}$. The numerical and steady solutions are shown by the solid and interrupted lines respectively.

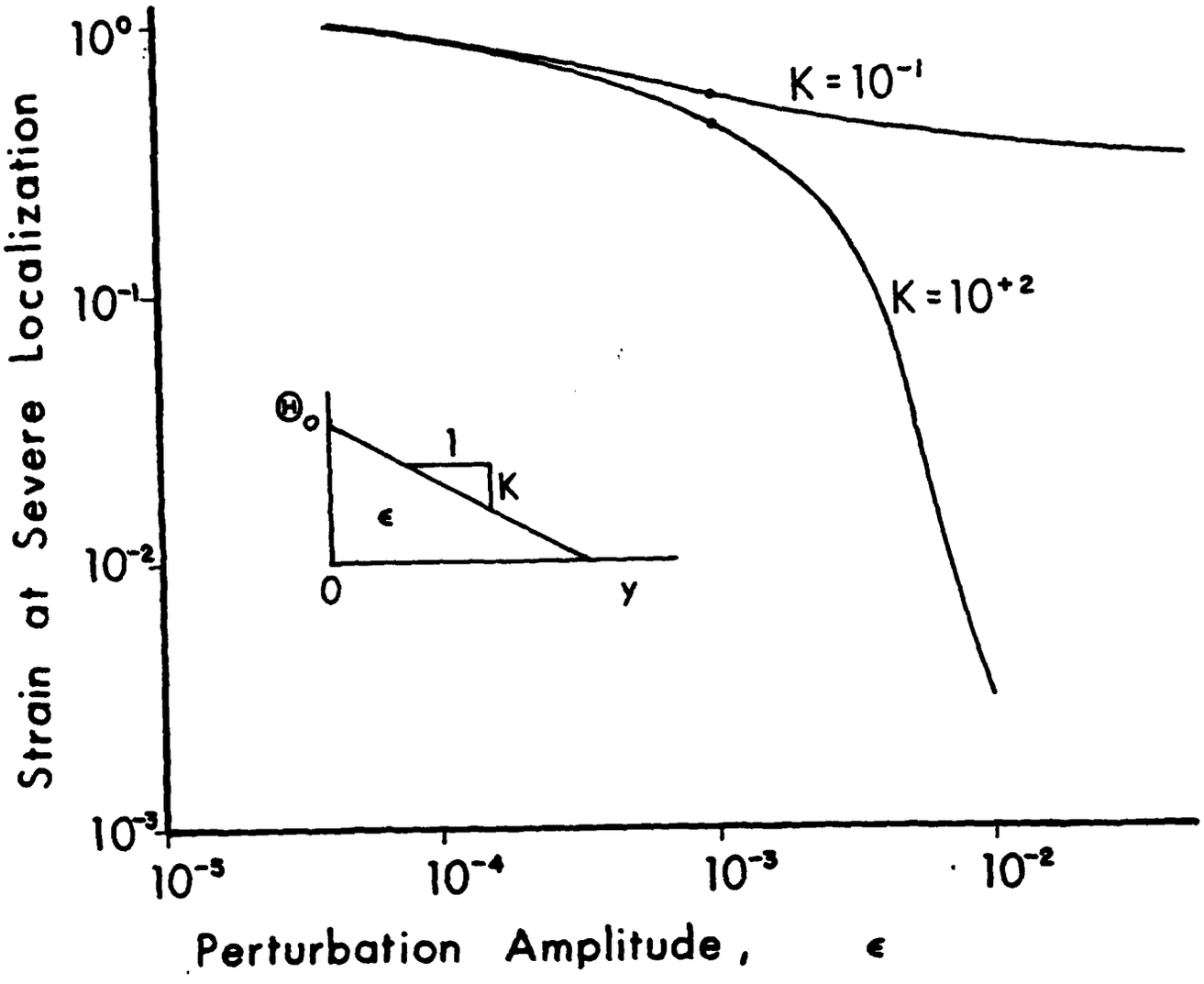

Figure 11. Critical strain at severe localization vs. perturbation amplitude with fixed triangular shape of the initial temperature perturbation.

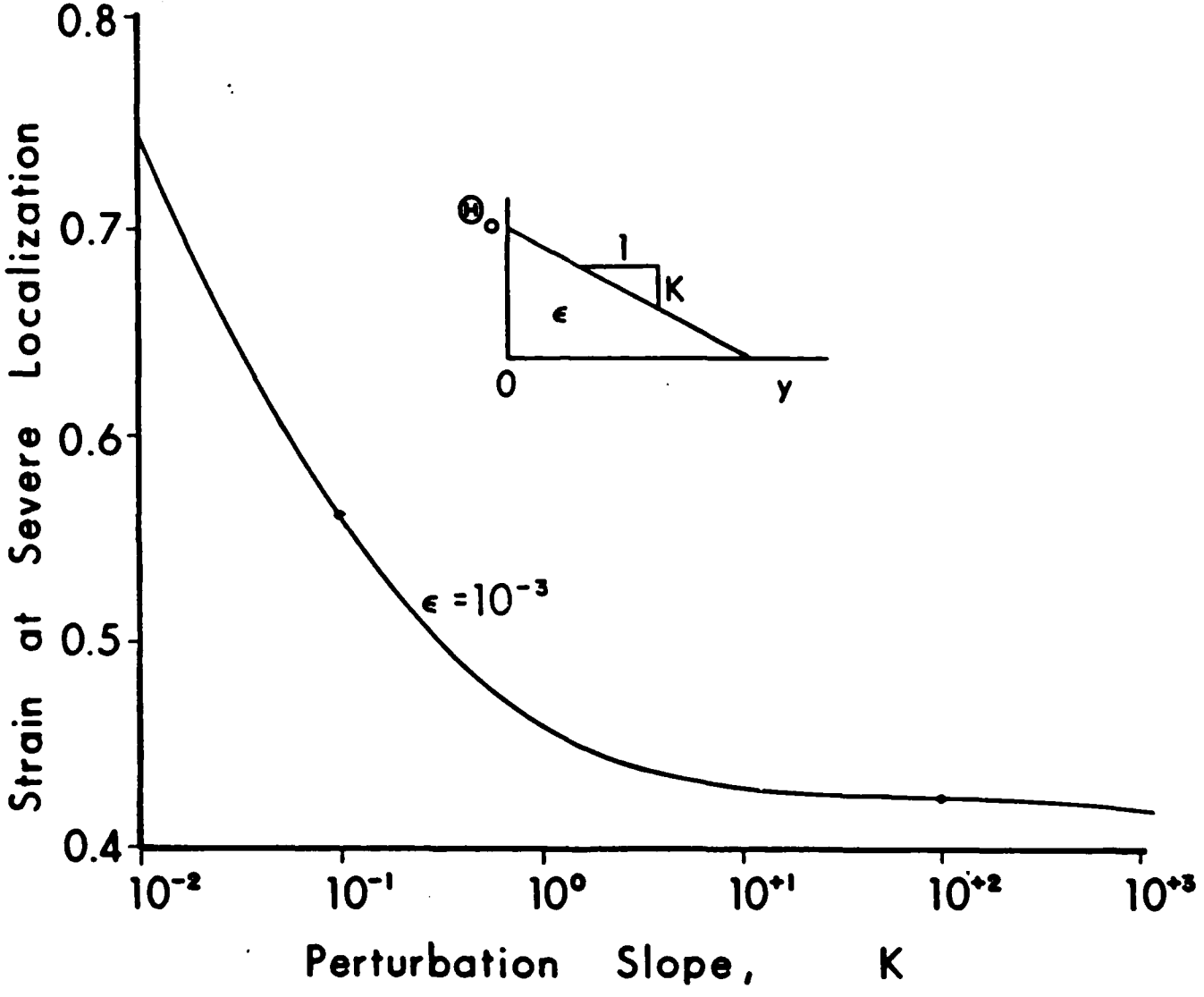

Figure 12. Critical strain at severe localization vs. slope of perturbation triangle with fixed area of the initial temperature perturbation.

broad and flat, and then early growth and later severe localization follow in much the same pattern for all K varying over three decades or more.

8. DISCUSSION AND CONCLUSIONS

Adiabatic shear band formation is a major damage mechanism in ductile materials that undergo rapid deformation processes such as those that occur in machining, cutting, and forming operations, as well as during impact and penetration. The damage may occur locally along a plane, as in cutting or punching, or it may appear in a more or less distributed fashion, as in penetration, but in any case, it results in a reduction of shearing forces that can be transmitted through the material and ultimately in total failure. In this paper, the intent has been to clarify the dynamics of adiabatic shear band formation by studying a model that is simple enough for clarity, but that still represents the essential physics.

Even though the model is simple, it still requires five nondimensional constants, three of which contain the nominal or applied strain rate, $\dot{\gamma}_o$, and two of which contain the characteristic external length, H. In addition, the size and form of the perturbation introduces other parameters. From the mathematical point of view, it is generally most useful to examine influences on the solution due to variation of one nondimensional parameter at a time, but often such variation is not physically realizable, as in the present case. Here the primary variation studied was in the nominal strain rate, $\dot{\gamma}_o$, which enters into the nondimensional density, diffusivity, and one of the rate constants. However, for most of the cases analyzed, neither the density, which is extremely small, nor the rate constant, b, which is extremely large, have any appreciable effect on the major features of the solution. Thus, apart from a few calculations with limited variations of the size and form of the perturbation, the principal effects studied may be regarded as due to variation of the nondimensional diffusivity, k. The influence of the other parameters remains to be studied. Experience to date indicates that m and a will most likely have substantial influence on the timing of severe localization.

All results presented in this paper have assumed insulated boundaries. A few calculations were also made with the boundaries assumed to be held at constant temperature. The results differed scarcely at all from those presented above, except at points very close to the boundary where there was a rapid transition from a region of uniform temperature, whose value was virtually the same as that reached at the insulated boundary at an identical time. Thus, in this case, two boundary layers develop, one at the outer boundary and one in the center of the shear band. Of course, if the external dimension, H, is small enough, the two layers will overlap and interfere with each other, but that is another problem not considered here.

The numerical and asymptotic analyses in this paper show clearly that the early growth of a perturbation is only a precursor to intense localization, which occurs somewhat later. This is the single most important conclusion, which had been suggested by earlier calculations, but which here is definitive. The delay seems to be strongly affected by viscous stresses, perhaps in a manner analogous to that which occurs in viscous necking, as described by Hutchinson and Neale.[14]

LIST OF REFERENCES

1. Zener, C. and Holloman, J. H., 1944, Effect of Strain Rate upon Plastic Flow of Steel, J. Appl. Phys. 15, 22-32.

2. Rubin, D. and Drucker, D. C., 1969, On Stability of Viscoplastic Systems with Thermo-Mechanical Coupling, in Contributions to Mechanics, Markus Reiner 80th Anniversary Volume, ed. Abir, D., Pergamon Press, Oxford, London.

3. Clifton, R. J., 1980, Adiabatic Shear Banding, Chap. 8 in Materials Response to Ultra-High Loading Rates, ed. W. Herrmann, NRC Rept. NMAB-356.

4. Clifton, R. J., Duffy, J., Hartley, K. A., and Shawki, T. G., 1984, On Critical Conditions for Shear Band Formation at High Strain Rates, Scripta Met. 18, 443-448.

5. Bai, Y. -L., 1982, Thermo-Plastic Instability in Simple Shear, J. Mech. Phys. Sol. 30, 195-207.

6. Burns, T. J., 1985, Approximate Linear Stability Analysis of a Model of Adiabatic Shear Band Formation, Quart. App. Math. 43, 65-84.

7. Wright, T. W. and Batra, R. C., 1985, The Initiation and Growth of Adiabatic Shear Bands, Int. J. Plasticity 1, 205-212.

8. Wright, T. W. and Batra, R. C., 1985, Further Rersults on the Initiation and Growth of Adiabatic Shear Bands at High Strain Rates, J. de Physique 446, Coll. C5, Suppl. to No. 8, C5-323 to C5-330.

9. Wright, T. W. and Batra, R. C., 1986, Adiabatic Shear Bands in Simple and Dipolar Plastic Materials, to appear, IUTAM Symposium on Macro- and Micro-Mechanics of High Velocity Deformation and Fracture, ed. K. Kawata, Tokyo 1985.

10. Merzer, A. M., 1983, Modeling of Adiabatic Shear Band Development from Small Imperfections, J. Mech. Phys. Sol. 30, 323-338.

11. Wright, T. W., 1987, Steady Shearing in a Viscoplastic Solid, to appear, J. Mech. Phys. Sol.

12. Gear, C. W., 1971, Numerical Initial Value Problems in Ordinary Differential Equations, Prentice-Halll, Englewood Cliffs, New Jersey.

13. IMSL, 1985, User's Manual, IMSL Libaray, Edition 9.2, IMSL, Inc., Houston, Texas.

14. Hutchinson, J. W., and Neale, K. W., 1977, Influence of Strain-Rate Sensitivity on Necking under Uniaxial Tension, Acta Meet. 25, 839-846.

DISTRIBUTION LIST

No. of Copies	Organization
12	Administrator Defense Technical Info Center ATTN: DTIC-FDAC Cameron Station, Bldg 5 Alexandria, VA 22304-6145
4	Director Defense Advanced Research Projects Agency ATTN: Tech Info Dr. E. Van Reuth Dr. G. Farnum Dr. B. Wilcox 1400 Wilson Boulevard Arlington, VA 22209
1	Deputy Assistant Secretary of the Army (R&D) Department of the Army Washington, DC 20310
1	HQDA DAMA-ART-M Washington, DC 20310
1	C.I.A. OIR/DB/Standard GE47 HQ Washington, DC 20505
1	Commander U.S. Army War College ATTN: Lib Carlisle Barracks, PA 17013
1	Commander U.S. Army Command and General Staff College ATTN: Archives Fort Leavenworth, KS 66027
1	Commander U.S. Army Materiel Command ATTN: AMCDRA-ST 5001 Eisenhower Avenue Alexandria, VA 22333-0001
1	Commander U.S. Army Armament Research, Development and Engineering Center ATTN: SMCAR-LCA, T. Davidson Dover, NJ 07801-5001
3	Commander U.S. Army Armament Research, Development and Engineering Center ATTN: SMCAR-SC, J. D. Corrie J. Beetle E. Bloore Dover, NJ 07801-5001
1	Commander U.S. Army ARDEC ATTN: SMCAR-TDC Dover, NJ 07801
1	Commander U.S. Army Armament Research, Development and Engineering Center ATTN: SMCAR-MSI Dover, NJ 07801-5001
1	Commander Benet Weapons Laboratory ATTN: Dr. E. Schneider Watervliet, NY 12189
1	Director U.S. AMCCOM ARDEC CCAC Benet Weapons Laboratory ATTN: SMCAR-CCB-TL Watervliet, NY 12189-4050
1	Commander U.S. Army Armament, Munitions and Chemical Command ATTN: AMSMC-IMP-L Rock Island, IL 61299-7300

DISTRIBUTION LIST

No. of Copies	Organization
1	Commander U.S. Army Aviation Systems Command ATTN: AMSAV-ES 4300 Goodfellow Boulevard St. Louis, MO 63120-1798
1	Director U.S. Army Aviation Research and Technology Activity Ames Research Center Moffett Field, CA 94035-1099
1	Commander U.S. Army Communications - Electronics Command ATTN: AMSEL-ED Fort Monmouth, NJ 07703-5301
1	Commander CECOM R&D Technical Library ATTN: AMSEL-IM-L (Reports Section) B.2700 Fort Monmouth, NJ 07703-5000
1	Commander U.S. Army Harry Diamond Laboratory ATTN: SLCHD-TA-L 2800 Powder Mill Road Adelphi, MD 20783
1	Commander MICOM Research, Development and Engineering Center ATTN: AMSMI-RD Redstone Arsenal, AL 35898-5500
1	Director Missile and Space Intelligence Center ATTN: AIAM-S-YDL Redstone Arsenal, AL 35898-5500
3	Director BMD Advanced Technology Center ATTN: ATC-T, M. Capps ATC-M, S. Brockway ATC-RN, P. Boyd P.O. Box 1500 Huntsville, AL 35807
2	Commander U.S. Army Mobility Equipment Research & Development Command ATTN: DRDME-WC DRSME-RZT Fort Belvoir, VA 22060
1	Commander U.S. Army Natick Research and Development Center ATTN: DRXRE, Dr. D. Sieling Natick, MA 01762
1	Commander U.S. Army Tank Automotive Command ATTN: AMSTA-TSL Warren, MI 48397-5000
1	Commander USAG ATTN: Technical Library Fort Huachuca, AZ 85613-6000
1	Commander U.S. Army Development and Employment Agency ATTN: MODE-ORO Fort Lewis, WA 98433
3	Commander U.S. Army Laboratory Command Materials Technology Laboratory ATTN: SLCMT-T, J. Mescall SLCMT-T, R. Shea SLCMT-H, S.C. Chou Watertown, MA 02172-0001

DISTRIBUTION LIST

No. of Copies	Organization
1	Director U.S. Army TRADOC Analysis Center ATTN: ATOR-TSL White Sands Missile Range, 88002-5502
1	Commandant U.S. Army Infantry School ATTN: ATSH-CD-CS-OR Fort Benning, GA 31905-5400
1	Director U.S. Army Advanced BMD Technology Center ATTN: CRDABH-5, W. Loomis P. O. Box 1500, West Station Huntsville, AL 35807
3	Commander U.S. Army Research Office ATTN: Dr. E. Saibel Dr. G. Meyer Dr. J. Chandra P. O. Box 12211 Research Triangle Park, NC 27709
2	Commander U.S. Army Research and Standardization Group (Europe) ATTN: Dr. J. Wu Dr. F. Oertel Box 65 FPO NY 09510
3	Office of Naval Research Department of the Navy ATTN: Dr. Y. Rajapakse Dr. A. Tucker Dr. A. Kushner Washington, DC 20360
3	Commander U.S. Naval Air Systems Command ATTN: AIR-604 Washington, DC 20360
1	Commander Naval Sea Systems Command ATTN: Code SEA 62D Department of the Navy Washington, DC 20362-5101
3	Commander Naval Surface Weapons Center ATTN: Dr. W. H. Holt Dr. W. Mock Tech Lib Dahlgren, VA 22448-5000
3	Commander Naval Surface Weapons Center ATTN: Dr. R. Crowe Code R32, Dr. S. Fishman Code X211, Lib Silver Spring, MD 20902-5000
1	Commander and Director US Naval Electronics Laboratory San Diego, CA 92152
5	Air Force Armament Laboratory ATTN: AFATL/DOIL (Tech Info Center) J. Foster John Collins Joe Smith Guy Spitale Eglin AFB, FL 32542-5438
1	RADC (EMTLD, Lib) Griffiss AFB, NY 13440
1	AUL (3T-AUL-60-118) Maxwell AFB, AL 36112

DISTRIBUTION LIST

No. of Copies	Organization
1	Air Force Wright Aeronautical Laboratories Air Force Systems Command Materials Laboratory ATTN: Dr. Theodore Nicholas Wright-Patterson AFB, OH 45433
1	Air Force Wright Aeronautical Laboratories Air Force Systems Command Materials Laboratory ATTN: Dr. John P. Henderson Wright-Patterson AFB, OH 45433
1	Director Environmental Science Service Administration US Department of Commerce Boulder, CO 80302
1	Director Lawrence Livermore Laboratory ATTN: Dr. M. L. Wilkins P. O. Box 808 Livermore, CA 94550
8	Sandia National Laboratories ATTN: Dr. L. Davison Dr. P. Chen Dr. L. Bertholf Dr. W. Herrmann Dr. J. Nunziato Dr. S. Passman Dr. E. Dunn Dr. M. Forrestal P. O. Box 5800 Albuquerque, NM 87185-5800
1	Sandia National Laboratories ATTN: Dr. D. Bamman Livermore, CA 94550
1	Director National Aeronautics and Space Administration Lyndon B. Johnson Space Center ATTN: Lib Houston, TX 77058
1	Director Jet Propulsion Laboratory ATTN: Lib (TDS) 4800 Oak Grove Drive Pasadena, CA 91103
1	National Bureau of Standards ATTN: Dr. Timothy Burns Technology Building, Rm A151 Gaithersburg, MD 20899
1	A.R.A.P. Group, Titan Systems, Inc. ATTN: Ray Gogolewski 1800 Old Meadow Rd., #114 McLean, VA 22102
1	ETA Corporation ATTN: Dr. D. L. Mykkanen P. O. Box 6625 Orange, CA 92667
1	Forestal Research Center Aeronautical Engineering Lab. Princeton University ATTN: Dr. A. Eringen Princeton, NJ 08540
1	Honeywell, Inc. Defense Systems Division ATTN: Dr. Gordon Johnson 600 Second Street, NE Hopkins, MN 55343

DISTRIBUTION LIST

No. of Copies	Organization
2	Orlando Technology, Inc. ATTN: Dr. Daniel Matuska Dr. John J. Osborn P. O. Box 855 Shalimar, FL 32579
6	SRI International ATTN: Dr. Donald R. Curran Dr. Donald A. Shockey Dr. Lynn Seaman Mr. D. Erlich Dr. A. Florence Dr. R. Caligiuri 333 Ravenswood Avenue Menlo Park, CA 94025
1	Systems Planning Corporation ATTN: Mr. T. Hafer 1500 Wilson Boulevard Arlington, VA 22209
1	Terra-Tek, Inc. ATTN: Dr. Arfon Jones 420 Wahara Way University Research Park Salt Lake City, UT 84108
2	California Institute of Technology Division of Engineering and Applied Science ATTN: Dr. E. Sternberg Dr. J. Knowles Pasadena, CA 91102
1	Denver Research Institute University of Denver ATTN: Dr. R. Recht P. O. Box 10127 Denver, CO 80210
1	Massachusetts Institute of Technology ATTN: Dr. R. Probstein 77 Massachusetts Avenue Cambridge, MA 02139
1	Massachusetts Institute of Technology Department of Mechanical Engineering ATTN: Prof. L. Anand Cambridge, MA 02139
3	Rensselaer Polytechnic Institute ATTN: Prof. E. H. Lee Prof. E. Krempl Prof. J. Flaherty Troy, NY 12181
1	Southwest Research Institute Department of Mechanical Sciences ATTN: Dr. U. Lindholm 8500 Culebra Road San Antonio, TX 78228
5	Brown University Division of Engineering ATTN: Prof. R. Clifton Prof. H. Kolsky Prof. L. B. Freund Prof. A. Needleman Prof. R. Asaro Providence, RI 02912
1	Brown University Division of Applied Mathematics ATTN: Prof. C. Dafermos Providence, RI 02912
3	Carnegie-Mellon University Department of Mathematics ATTN: Dr. D. Owen Dr. M. E. Gurtin Dr. B. D. Coleman Pittsburgh, PA 15213

DISTRIBUTION LIST

No. of Copies	Organization
6	Cornell University Department of Theoretical and Applied Mechanics ATTN: Dr. Y. H. Pao Dr. A. Ruoff Dr. J. Jenkins Dr. R. Lance Dr. F. Moon Dr. E. Hart Ithaca, NY 14850
2	Harvard University Division of Engineering and Applied Physics ATTN: Prof. J. R. Rice Prof. J. Hutchinson Cambridge, MA 02138
2	Iowa State University Engineering Research Laboratory ATTN: Dr. A. Sedov Dr. G. Nariboli Ames, IA 50010
2	Lehigh University Center for the Application of Mathematics ATTN: Dr. E. Varley Dr. R. Rivlin Bethlehem, PA 18015
1	New York University Department of Mathematics ATTN: Dr. J. Keller University Heights New York, NY 10053
1	North Carolina State University Department of Civil Engineering ATTN: Prof. Y. Horie Raleigh, NC 27607
1	Pennsylvania State University Engineering Mechanical Dept. ATTN: Prof. N. Davids University Park, PA 16502
1	Rice University ATTN: Dr. C. C. Wang P. O. Box 1892 Houston, TX 77001
1	Southern Methodist University Solid Mechanics Division ATTN: Prof. H. Watson Dallas, TX 75221
1	Temple University College of Engineering Tech. ATTN: Dr. R. Haythornthwaite Dean Philadelphia, PA 19122
5	The Johns Hopkins University ATTN: Prof. R. B. Pond, Sr. Prof. R. Green Prof. W. Sharpe Prof. J. F. Bell Prof. C. A. Truesdell 34th and Charles Streets Baltimore, MD 21218
1	Tulane University Department of Mechanical Engineering ATTN: Dr. S. Cowin New Orleans, LA 70112
3	University of California Department of Mechanical Engineering ATTN: Dr. M. Carroll Dr. W. Goldsmith Dr. P. Naghdi Berkeley, CA 94704

DISTRIBUTION LIST

No. of Copies	Organization
1	University of California Dept of Aerospace and Mechanical Engineering Science ATTN: Dr. Y. C. Fung P. O. Box 109 La Jolla, CA 92037
1	University of California Department of Mechanics ATTN: Dr. R. Stern 504 Hilgard Avenue Los Angeles, CA 90024
1	University of California at Santa Barbara Department of Mechanical Engineering ATTN: Prof. T. P. Mitchel Santa Barbara, CA 93106
1	University of California at Santa Barbara Department of Materials Science ATTN: Prof. A. G. Evans Santa Barbara, CA 93106
1	University of California at San Diego Department of Mechanical Engineering ATTN: Prof. S. Nemat Nassar La Jolla, CA 92093
2	University of Delaware Department of Mechanical and Aerospace Engineering ATTN: Dr. Minoru Taya Prof. J. Vinson Newark, DE 19711
4	University of Florida Department of Engineering Science and Mechanics ATTN: Prof. L. Malvern Prof. D. Drucker Prof. E. Walsh Prof. M. Eisenberg Gainesville, FL 32601
2	University of Houston Department of Mechanical Engineering ATTN: Dr. T. Wheeler Dr. R. Nachlinger Houston, TX 77004
2	University of Illinois Department of Theoretical and Applied Mechanics ATTN: Dr. D. Carlson Prof. D. Scott Stewart Urbana, IL 61801
2	University of Illinois at Chicago Circle College of Engineering Department of Engineering, Mechanics, and Metallurgy ATTN: Prof. T.C.T. Ting Prof. D. Krajcinovic P. O. Box 4348 Chicago, IL 60680
2	University of Kentucky Department of Engineering Mechanics ATTN: Dr. M. Beatty Prof. O. Dillon, Jr. Lexington, KY 40506
1	University of Kentucky School of Engineering ATTN: Dean R. M. Bowen Lexington, KY 40506

DISTRIBUTION LIST

No. of Copies	Organization
2	University of Maryland Department of Mathematics ATTN: Prof. S. Antman Prof. T. P. Liu College Park, MD 20742
3	University of Minnesota Department of Engineering Mechanics ATTN: Prof. J. L. Erickson Prof. R. Fosdick Prof. R. James Minneapolis, MN 55455
1	University of Missouri-Rolla Department of Engineering Mechanics ATTN: Prof. R. C. Batra Rolla, MO 65401-0249
2	University of Oklahoma School of Aerospace, Mechanical and Nuclear Engineering ATTN: Prof. Akhtar S. Khan Prof. Charles W. Bert Norman, Oklahoma 73019
1	University of Pennsylvania Towne School of Civil and Mechanical Engineering ATTN: Prof. Z. Hashin Philadelphia, PA 19105
4	University of Texas Department of Engineering Mechanics ATTN: Dr. M. Stern Dr. M. Bedford Prof. Ripperger Dr. J. T. Oden Austin, TX 78712
1	University of Washington Department of Aeronautics and Astronautics ATTN: Dr. Ian M. Fyfe 206 Guggenheim Hall Seattle, WA 98195
1	University of Wyoming Department of Mathematics ATTN: Prof. R. E. Ewing P. O. Box 3036 University Station Laramie, WY 82070
3	Washington State University Department of Physics ATTN: Prof. R. Fowles Prof. G. Duvall Prof. Y. Gupta Pullman, WA 99163
2	Yale University ATTN: Dr. B.-T. Chu Dr. E. Onat 400 Temple Street New Haven, CT 96520

Aberdeen Proving Ground

Dir, USAMSAA
ATTN: AMXSY-D
AMXSY-MP, H. Cohen
Cdr, USATECOM
ATTN: AMSTE-SI-F
Cdr, CRDC, AMCCOM
ATTN: SMCCR-RSP-A
SMCCR-MU
SMCCR-SPS-IL

The following is an internal distribution list for the manuscript entitled,

On Stress Collapse in Adiabatic Shear Band

, written by Thomas W. Wright and John W. Walter.

NAME	DIVISION	NO. COPIES
Dr. C. Kitchens	TBD	1
Dr. A. Dietrich	TBD	1
Dr. T. Wright	TBD	1
Mr. R. Franz	TBD	1
Mr. G. Hauver	TBD	1
Mr. P. Netherwood	TBD	1
Dr. W. Bruchey	TBD	1
Dr. J. Zukas	TBD	1
Dr. G. Filbey	TBD	1
Dr. W. Gillich	TBD	1
Dr. N. Huffington	TBD	1
Dr. D. Haskell	VLD	1
Mr. R. Benck	TBD	1
Dr. W. deRosset	TBD	1
Mr. K. Frank	TBD	1
Dr. F. Grace	TBD	1
Dr. J. Santiago, Jr.	TBD	1
Mr. J. Suckling	VLD	1
Dr. P. Howe	TBD	1
Dr. R. Frey	TBD	1
Mr. J. Kineke, Jr.	TBD	1
Mr. W. Walters	TBD	1
Mr. H. Jonas	TBD	1
Mr. E. Rapacki, Jr.	TBD	1
Mr. W. Lawrence	TBD	1
Mr. D. Pritchard	TBD	1
Dr. P. Kingman	TBD	1
Ms. B. Ringers	TBD	1
Dr. W. Drysdale	IBD	1
Dr. D. Kooker	IBD	1
Dr. B. Burns	IBD	1
Dr. R. Lieb	IBD	1
Mr. J. Pilcher	IBD	1
Dr. D. Eccleshall	BMD	1
Dr. M. Scheidler	TBD	1
Dr. J. Walter	TBD	1

END

DATE

FILMED

FEB.

1988